Taylor & Francis
Taylor & Francis Group

Journal of Microencapsulation
Micro and Nano Carriers

ISSN: 0265-2048 (Print) 1464-5246 (Online) Journal homepage: www.tandfonline.com/journals/imnc20

siRNA-guided dual-targeting nanocarrier for breast cancer treatment

Ebru Kilicay, Betul Sahin, Zeynep Karahaliloglu, Ekin Celik & Baki Hazer

To cite this article: Ebru Kilicay, Betul Sahin, Zeynep Karahaliloglu, Ekin Celik & Baki Hazer (2025) siRNA-guided dual-targeting nanocarrier for breast cancer treatment, Journal of Microencapsulation, 42:5, 437-458, DOI: 10.1080/02652048.2025.2490041

To link to this article: https://doi.org/10.1080/02652048.2025.2490041

JOURNAL OF MICROENCAPSULATION
2025, VOL. 42, NO. 5, 437–458
https://doi.org/10.1080/02652048.2025.2490041

Taylor & Francis
Taylor & Francis Group

RESEARCH ARTICLE

siRNA-guided dual-targeting nanocarrier for breast cancer treatment

Ebru Kilicay[a], Betul Sahin[b], Zeynep Karahaliloglu[c], Ekin Celik[d] and Baki Hazer[e,f]

[a]Department of Medical Laboratory Techniques, Şabanözü Vocational School, Cankiri Karatekin University, Cankiri, Turkey; [b]Department of Chemistry, Graduate School of Natural and Applied Sciences, Cankiri Karatekin University, Cankiri, Turkey; [c]Biology Department, Faculty of Science and Arts, Aksaray University, Aksaray, Turkey; [d]Medical Biology Department, Faculty of Medicine, Ahi Evran University, Kırşehir, Turkey; [e]Department of Aircraft Airframe Engine Maintenance, Kapadokya University, Nevşehir, Turkey; [f]Department of Chemistry, Zonguldak Bülent Ecevit University, Zonguldak, Turkey

ABSTRACT

Aims: This study aimed to develop a thermoplastic polyurethane-oleic acid-based nanosystem (TPU-Ole NPs) incorporating siRNA and curcumin (CUR) to overcome multidrug resistance in breast cancer by silencing the c-myc gene.

Methods: TPU-Ole and CUR-loaded NPs were prepared via solvent evaporation and coated with poly-L-lysine (PLL) for siRNA attachment. NPs were characterised by dynamic light scattering (DLS) for mean diameter, polydispersity index (PDI), and zeta potential (ZP). Encapsulation (EE) and loading efficiencies (LE) were measured by NanoDrop. Release (pH 5.0; 7.4) and storage stability (pH 7.4) were evaluated using the eppendorf method. siRNA binding was confirmed by agarose gel electrophoresis. Gene silencing and apoptosis were assessed by RT-PCR and flow cytometry.

Results: Mean diameter, PDI, and ZP of NPs were 170 ± 2 nm, 0.011 ± 0.080, and −27.5 ± 0.11 mV. EE and LE were 75 ± 0.12 and 14.2 ± 0.06%. Sustained release and good stability were observed.

Conclusion: siRNA-CUR-NPs efficiently silenced c-myc and induced apoptosis in MCF-7 cells.

ARTICLE HISTORY
Received 3 May 2024
Accepted 3 April 2025

KEYWORDS
Thermoplastic polyurethane; oleic acid; curcumin; siRNA; L929; MCF-7

1. Introduction

Breast cancer is the most common malignancy among women worldwide, with the highest mortality rate. Its treatment remains challenging due to molecular complexity, high relapse risk, rapid metastasis, chemotherapy resistance, and tumour heterogeneity (Chadar and Kesharvani 2021). Traditional treatments, such as surgery, radiotherapy, and systemic therapies (chemotherapy, hormone, and targeted therapy) often suffer from low selectivity, multidrug resistance, and non-specific drug distribution (Dongsar *et al.* 2023). Additionally, chemotherapeutic agents like paclitaxel, docetaxel, doxorubicin exhibit limitations due to poor solubility, low bioavailability, and non-selective cytotoxicty. Moreover, rapid clearance, toxicity to healthy tissues and poor tumour targeting further hinder their therapeutic efficacy (Ashrafizadeh *et al.* 2020). To address these challenges, targeted delivery systems have been developed. One promising approach is gene therapy via RNA interference (RNAi).

RNAi is a natural gene-silencing mechanism in which small interfering RNA (siRNA**)** degrades specific mRNA sequences, preventing translation into proteins. siRNA has been extensively investigated for its potential to silence oncogenes, including c-myc, a key driver of cancer progression (Hanafi-Boid *et al.* 2016).

Cancer arises from a cascade of genetic mutations, including oncogene activation and tumour suppressor gene loss, leading to uncontrolled proliferation and impaired apoptosis (McLeod 2013, Suvà *et al.* 2013, Lee *et al.* 2016). Among the identified driver genes (Walther and Schlag 2013, Farooqi *et al.* 2014), MYC is one of the most crucial oncogenes in tumorigenesis. Overexpression of c-Myc enhances tumour aggressiveness by disrupting cell cycle regulation, altering chromatin structure, and promoting angiogenesis (Lin *et al.* 2012).

siRNA-based therapies hold significant promise in cancer treatment by selectively targeting oncogenes (Elbashir *et al.* 2001, Bora *et al.* 2012). However, due to the complexity of cancer-related gene dysregulation, siRNA alone is often insufficient for effective treatment. Combining siRNA with chemotherapeutic agents can enhance treatment efficacy. Natural compounds, such as curcumin (CUR), a polyphenolic component of

CONTACT Ebru Kilicay ebru.kilicay@gmail.com Department of Medical Laboratory Techniques, Şabanözü Vocational School, Cankiri Karatekin University, Cankiri, Turkey

Supplemental data for this article can be accessed online at https://doi.org/10.1080/02652048.2025.2490041.

Curcuma longa, have demonstrated potent anticancer effects through anti-inflammatory, antioxidant, and apoptosis-inducing mechanisms (Medel *et al*. 2017, Saleh *et al*. 2019, Kim *et al*. 2023). Despite its therapeutic potential, CUR suffers from poor water solubility and low bioavailability, necessitating innovative drug delivery strategies to enhance stability, solubility, and efficacy.

Nano-drug delivery systems have gained increasing attention for overcoming these shortcomings, as they can improve the therapeutic index of drugs. However, drug resistance in cancer cells can limit the effectiveness of these therapies. Despite the combination of chemotherapeutic agents to prevent drug resistance in cancer patients, cancer cells can adapt to one or more drugs and resistance pathways may develop, leading to treatment failure in various types of cancer (Gottesman 2002). Novel approaches aim to overcome drug resistance through nanocarrier based delivery systems, which facilitate endosomal release of chemotherapeutic agents (Chow *et al*. 2011). Additionally, the release of nucleic acids (e.g. siRNA) from nanocarriers enables the silencing of genes involved in drug resistance (Meng *et al*. 2013). siRNA targets specific genes that prevent apoptosis or promote cell division, but it cannot be used as a single therapy due to the multiple gene dysregulations observed in cancer (Qian *et al*. 2015, Young *et al*. 2016).

A single nanocarrier system integrating siRNA with chemotherapeutic agents can exert strong synergistic effects by simultaneously inducing cytotoxicity and suppressing oncogene expression (Suo *et al*. 2017, Sun *et al*. 2018). In addition, nanocarriers can escape from multidrug resistance efflux by entering tumour cells through endocytic pathways (Mirza and Karim 2021). Therefore, the double synergistic combination of anticancer agent and siRNA integrated into nano-sized carrier systems present a highly effective treatment strategy.

In one study, Zhang and research group developed lipid/calcium/phosphate (LCP) nanoparticles to treat aggressive small lung cancer cells using a combination of chemotherapy and gene therapy. The chemodrug gemcitabine monophosphate (GMP) and c-myc oncogene-specific siRNA were encapsulated into the nano-carrier and administered to mice. Tumour cell apoptosis was observed when either c-myc siRNA or GMP was used alone. However, the combination therapy significantly inhibited tumour growth (Zhang *et al*. 2013).

Reliable and efficient gene nanocarrier systems are crucial for gene therapy applications. Cationic polymers, such as poly-L-lysine (PLL), polyethyleneimine (PEI), and their derivates have gained attention for gene delivery due to their strong binding affinity to nucleic acids, biocompatibility, ease of modification, and large scale production. Non-viral vectors are widely used for these applications. Among them, thermoplastic polyurethane (TPU) and PLL have great potential for delivering genes to target cells.

Polyurethanes (PU) are known their excellent biocompatibility, mechanical properties, and synthetic versatility (Nair and Laurencin 2007). They are widely used in biomedical applications, such as prosthetic heart valves, drug and gene delivery systems (Mahdieh *et al*. 2024), catheters, blood pumps, and dressing materials (Vermette *et al*. 2001). PLL, a biodegradable and biocompatible cationic polypeptide, can efficiently bind to negatively charged molecules, such as DNA through electrostatic interactions, making it an excellent candidate for nucleic acid and drug delivery.

A notable example of a gene carrier nanosystem was reported by Liu *et al*. They synthesised amphiphilic block copolymer composed of monomethoxy (polyethylene glycol)-poly(D,L-lactide-co-glycolide)-poly(L-lysine) (mPEG-PLGA-b-PLL) and formulated NPs loaded with either the anti-cancer drug adriamycin or siRNA loaded NPs (mPEG-PLGA-b-PLL NPs). Flow cytometry analysis demonstrated that mPEG-PLGA-b-PLL NPs exhibited superior efficacy compared to the free drug in facilitating the targeted delivery of both adriamycin and siRNA in Huh-7 hepatic carcinoma-bearing mice. This enhanced performance was primarily attributed to the high cellular uptake of adriamycin and siRNA loaded mPEG-PLGA-b-PLL NPs. Consequently, these NPs exhibited great potential as effective carriers for adriamycin and siRNA (Liu *et al*. 2012).

Despite TPU has many advantages, its drug encapsulation efficiency can be limited when used alone. To overcome this drawback, oleic acid (Ole) can be incorporated into TPU, significantly improving its properties. Ole, a type of fatty acid, has been widely used as a hydrophobic pharmaceutical excipient in polymer synthesis due to their ability to improve mechanical and physicochemical properties (Barnwell and Attwood 1992, Yamashita *et al*. 1995, Kalhapure and Akamanchi 2012, Tran *et al*. 2017). Ole also demonstrates biocompatibility, biodegradability, and permeation enhancing effects (Omolo *et al*. 2017) and it is also used as an agent that provides high encapsulation efficiency and stability. Additionally, as a capping agent, Ole prevents the NP aggregation and facilitates integration with thermoplastic polymers (Patra *et al*. 2024). The incorporation of hydrophobic segments, such as Ole, stearic acid, linoleic acid, or cholesterol into siRNA delivery systems has greatly contributed to increase cellular uptake,

transfection efficiency, and endosomal release into the cytoplasm (Liu *et al.* 2010, Wang *et al.* 2011, Layek *et al.* 2014). Based on these properties of Ole, Tran *et al.* designed Ole and gelatine conjugated silica-coated iron oxide magnetic nanoparticles for diagnostic imaging and cancer therapy. This conjugation improved the solubility of the nanoparticles and facilitated the incorporation of hydrophobic drug into shell, enhancing anticancer efficiency through the controlled release of the encapsulated drug in both cellular and animal models. Following Ole-gelatine functionalization, the NPs showed a high loading capacity for the hydrophobic anticancer drug, paclitaxel. Therefore, this nanosystem could be a promising multifunctional platform for cancer therapy (Tran *et al.* 2017).

Inspired by these findings, this study aimed to develop a nanocarrier system that could overcome multidrug resistance by combining both the chemotherapeutic agent CUR and RNAi-based anticancer therapy for effective breast cancer treatment. To date, no study has reported the use of TPU-Ole polymer for enhancing the activity of therapeutic agents. The incorporation of Ole into polymeric NPs made this study more meaningful, unique, and effective. The TPU used demonstrated a high absorption capacity for targeting and the ability to cross biological barrier easily. Because of the potential of amphiphilic copolymers with amino acid ingredients for chemical agent and siRNA delivery, TPU-Ole polymer was synthesised, Subsequently, TPU-Ole NPs and siRNA conjugated-CUR loaded formulations were prepared using solvent evaporation technique. The *in vitro* efficiency of the co-delivery system, incorporating CUR and siRNA within PLL-TPU-Ole NPs (siRNA-CUR-TPU-Ole NPs), was evaluated in L929 mouse fibroblast cells and MCF-7 human breast cancer cells. As a result, c-myc-siRNA incorporated into CUR-TPU-Ole NPs demonstrated high transfection efficiency and significant anticancer activity for the treatment of breast cancer by suppressing the cmyc gene.

2. Materials and methods

2.1. Materials

TPU was purchased from BASF Company (Elastollan cod no: 1185A 10M). Chloroform, Tween-80, and curcumin (Mw = 368.38) were purchased from Merck (Darmstadt, Germany). PLL solution (P4707, mol wt 70 000–150 000) and other chemicals were obtained from Sigma-Aldrich. siRNA (Sens sequence: 5′CCGUGGAUCUGAAUUACAATT-3′; antisense sequence: 5′UUGUAAUUCAGAUCCACGGAA-3′) and HiperFect Transfection Reagent composed of a mixture of cationic and neutral lipid used as carrier were purchased from Qiagen (Germany). The MCF-7 and L929 were obtained from the American Type Culture Collection (Manassas, VA, USA). RPMI-1640, trypsin-EDTA, 10% foetal bovine serum (FBS), 1% penicillin/streptomycin, and dimethyl sulfoxide (DMSO) were purchased from Biological Industries (Beit Haemek, Israel). Ribonuclease A (RNase A) and Annexin V-FITC Apoptosis Detection Kit were purchased from Serva (USA). Phosphate buffered saline (PBS) was obtained from Thermo Scientific, USA.

2.2. The synthesis and characterisation of PU-oleic acid polymer

1.66 g of TPU (Figure 1(a)) and 2.61 g of Ole (85–88% purity by weight, (w/w)) (Hazer *et al.* 2019) were dissolved in a mixture of 11 ml of dimethylformamide (DMF) and 6.5 ml of tetrahydrofuran (THF) and poured into a petri dish ($\Phi = 9$ cm). This solution was then placed in an ordinary oven and kept at 130 °C for 1 h. The resulting TPU functionalised with Ole was quickly redissolved in the DMF/THF mixture and the TPU-Ole was poured into distilled water and precipitated. The obtained product was dried in a vacuum oven at 40 °C (Figure 1(b)) (Barick and Tripathy 2011). The –NH– group of the urethane was formed by the reaction of alcohol and isocyanate with the carboxylic acid of oleic acid. The molecular weight was determined by Gel Permeation Chromatography (GPC) (Agilent Brand, 7890A model G1888 Network Headspace Sampler, 16 Vial Autosampler, FID Detector) to confirm the formation of TPU-Ole. Fourier Transform Infra-red (FTIR) Spectroscopy (Perkin Elmer SpectrumOne, Nicolet 520, USA), Hydrogen Nuclear Magnetic Resonance (^{1}HNMR) (Agilent, Santa Clara, CA, USA), Differential Scanning Calorimetry (DSC) (Shimadzu DSC-60, Perkin Elmer Diamond, Houston, TX, USA), Thermogravimetric Analysis (TGA) (Shimadzu DTG-60, Perkin Elmer Pyris, Woodland, CA, USA) and X-Ray Diffraction (XRD) Analysis (Rigaku Tltima-IV X-Ray, Texas, USA) were also performed for the physicochemical characterisation of TPU-Ole polymer. The TPU-Ole polymer was extracted with THF using a Soxhlet apparatus and the acetone-washed polymer was analysed for residual content using Gas Chromatography-Mass Spectrometry (GC-MS).

2.3. Preparation and characterisation of TPU-Ole NPs and CUR-TPU-Ole NPs

TPU-Ole NPs were prepared using a single emulsion/solvent evaporation technique. For this, 10 mg of

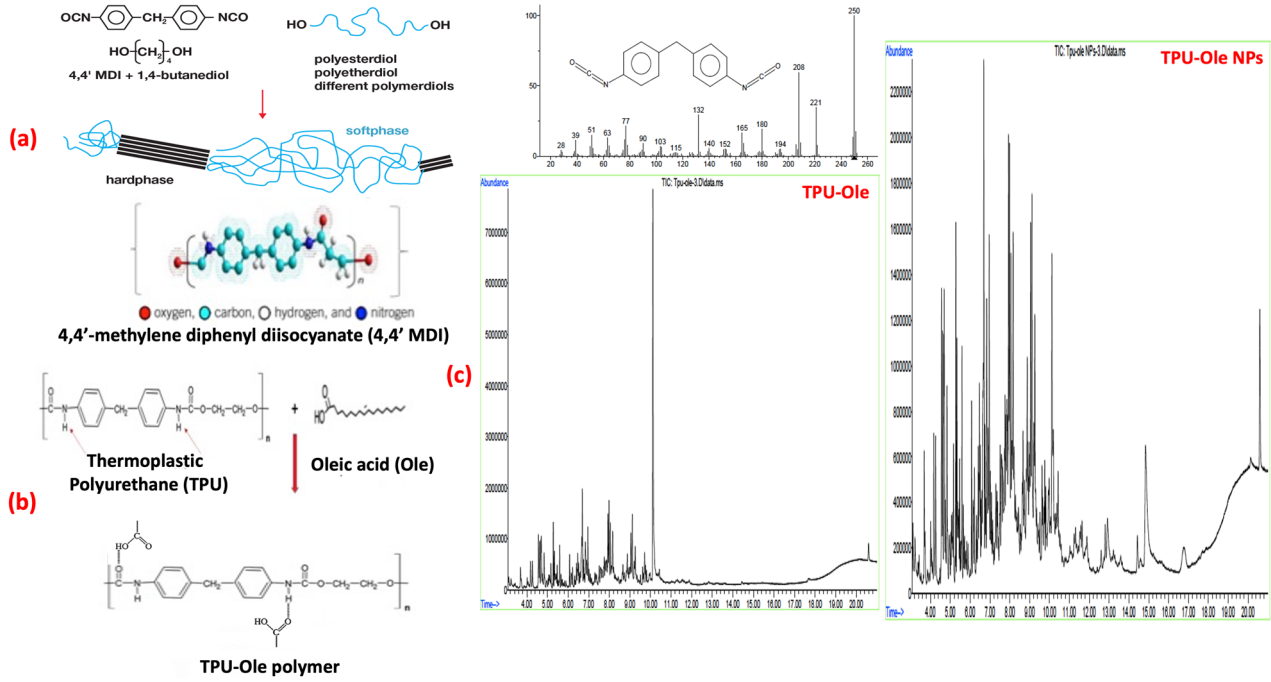

Figure 1. (a) Chemical structure of 4,4′-MDI, 4,4′-methyl diphenyl diisocyanate; (b) oleic acid doped TPU polymers (c) GC-MS spectra of TPU-Ole and TPU-Ole NPs. Mass spectrometry analysis confirmed the absence of residual in isocyanate in sample.

TPU-Ole polymer was dissolved in 10 ml of THF and injected dropwise into an aqueous dispersion medium containing Tween 80 (6%, v/v) as a surfactant, using a homogeniser (IKA T 125 Digital Ultra Turrax Homogeniser, Deutschland, Germany) and an ice bath (Mattu *et al.* 2013). The mixture was then stirred in the presence of an ultrasonic bath (Alex, Germany) and a mechanical stirrer (Heidolph RZR 2021, North America) at 2000 rpm/min to evaporate the solvent. The resulting suspension was centrifuged (Centrifuge 5810R) at 12 000 rpm for 30 min. The supernatant was discarded, and the remaining NPs were washed three times with distilled water to remove the unreacted organic solvent, polymer, and Tween 80. Zeta-Sizer (3000 HSA, Malvern, England) was used to evaluate the size-size distribution of the NPs. Once the optimal mean diameter of particles was achieved, all samples were lyophilised (Martin Christ GmbH, Osterode am Harz, Germany) at −80 °C and then stored at 4 °C for further experiments.

Scanning Electron Microscope (SEM), Transmission Electron Microscope (TEM) were used to evaluate the morphology. To assess the presence of isocyanate residues in the polymer and nanostructure, GC-MS analysis was performed using an Agilent 7890A GC-Agilent 5975C Inert MSD Model device. 50 mg of dry polymer and NPs were mixed with 1.5 ml of THF, vortexed at high speed, and incubated at room temperature overnight. The resulting solution was analysed without further processing.

CUR-NPs were prepared using the same emulsion/solvent evaporation method. TPU-Ole and CUR/ethanol solutions were dissolved in THF at different polymer to drug weight ratios: 1/0.25 TPU-Ole/CUR (2.5CUR-NPs) and 1/1 TPU-Ole/CUR (10CUR-NPs). The mixture was then separately poured into the dispersion medium and homogenised. The resulting CUR-NPs were lyophilised for subsequent experiments. FTIR spectroscopy of blank and CUR-NPs was taken. SEM and TEM were performed to examine surface morphology.

2.3.1. Determination of CUR loading and encapsulation efficiencies

The loading (LE) and encapsulation efficiency (EE) of CUR-NPs were measured by dispersing the aqueous suspensions of NPs, followed by centrifugation at 12 000 rpm for 30 min (Kilicay *et al.* 2016). The precipitated NPs were collected and lyophilised. To determine the amount of free CUR in the supernatant, the washing solutions were collected and the absorbance was measured at a wavelength of 428 nm using a Nanodrop (Thermo Scientific Nano Drop 1000 Spectrophotometer) (Meng *et al.* 2021). The necessary calculations were then performed using a CUR calibration curve.

2.4. Modification and characterisation of TPU-Ole NPs with PLL

PLL is a polar basic amino acid with a proton-accepting side chain at pH 7.4. To enable electrostatic interaction between the negatively charged siRNA and TPU-Ole, which also carries a negative charge, TPU-Ole NPs were functionalised with the PLL to confer a positive surface charge (Chevalier *et al.* 2017). A solution of 40 µg/ml TPU-Ole NPs was added to distilled water and stirred at room temperature for 1 h using a magnetic stirrer. PLL solutions (0.1% w/v in water) of 250 and 1000 µl (Anilmis *et al.* 2019) were separately added to the NP solution and stirred for 24 h to allow PLL binding to the NP surface. The following day, the mixture was centrifuged at 12 000 rpm for 15 min to remove unbound PLL. The surface charge and mean diameter of the resulting TPU-Ole NPs were measured using the Dynamic Light Scattering (DLS) to confirm the positive charge.

2.4.1. Conjugation and characterisation of PLL-TPU-Ole NPs and PLL-TPU-Ole-CUR NPs with c-myc siRNA

In this study, c-myc specific siRNA (Sense strain: 5′CCGUGGAUCUGAAUUACAATT-3′; antisense strain: 50UUGUAAUUCAGAUCCACGGAA-3′) was obtained from Qiagen. The lyophilised siRNA was diluted with RNase-free water. Different concentrations of siRNA were used to interact with PLL-TPU-Ole NPs to prepare siRNA-NPs (Yalcin *et al.* 2019). To achieve this, 5 and 15 µl of siRNA stock solutions were added to PLL-TPU-Ole NPs at concentrations of 40 and 120 µg/ml, respectively, to achieve siRNA concentrations of 100 and 600 nM (Anilmis *et al.* 2019, Yi *et al.* 2019). The resulting solution was then rotated at 15 rpm for 1 h to facilitate complex formation. Subsequently, the siRNA-NP solution was centrifuged at 12 000 rpm for 15 min to wash with distilled water. The same procedure was applied to CUR-NPs to obtain siRNA-CUR-TPU-Ole NPs. The mean diameter and zeta potential (ZP) of siRNA-PLL-TPU-Ole NPs and siRNA-PLL-CUR-TPU-Ole NPs were measured using DLS to confirm siRNA binding. All measurements were performed five times and the mean ± standard deviation (*SD*) was recorded for each sample.

2.4.2. Determination binding efficiency of siRNA

The suspensions of siRNA-TPU-Ole NPs and siRNA-CUR-TPU-Ole NPs were centrifuged at 12 000 rpm for 15 min and the supernatant was collected. The amount of unconjugated siRNA was quantified by measuring absorbance at 260 nm using a Nanodrop (Nanodrop 2000, Thermo Fisher Scientific) (Liu *et al.* 2012). A bare siRNA stock solution was used as a blank, and the siRNA binding efficiency for each NP formulation was calculated.

2.4.3. Agarose gel electrophoresis

Gel electrophoresis was performed to assess the binding and condensation capacity of siRNA on the surface of NPs. For this purpose, 10 µl of TPU-Ole NPs/siRNA and CUR-TPU-Ole NPs/siRNA were prepared at a weight ratio of 1:100 with a final concentration of 1.0 µg/ml. The samples were mixed with tris-acetate running buffer and electrophoresed at 100 V for 90 min on a 0.8% (w/v) agarose gel containing ethidium bromide (0.1 µg/ml). Naked siRNA (without NPs) diluted in the same buffer was used as a control to evaluate siRNA migration patterns (Wu *et al.* 2018).

2.5. Stability and in vitro release studies of siRNA-TPU-Ole NPs and siRNA-CUR-TPU-Ole NPs

The *in vitro* release profile was investigated using the Eppendorf method (Baby *et al.* 2021). For this, 100siRNA-TPU-Ole NPs, 600siRNA-TPU-Ole NPs, 100siRNA-2.5CUR-TPU-Ole NPs, 100siRNA-10CUR-TPU-Ole NPs, 600siRNA-2.5CUR-TPU-Ole NPs, and 600siRNA-10CUR-TPU-Ole NPs were placed in separate Eppendorf tubes, diluted in PBS (pH 7.4 and 5.0) (Wang *et al.* 2013a, 2013c, Sun *et al.* 2018, Yadav *et al.* 2018) and incubated at 37 °C in a shaking water bath (60 rpm). Absorbance measurements were recorded at 0.5, 1, 2.5, 3, 3.5, 4, 4.5, 5, 7, 10, 12, 24, and 48 h, followed by additional time points up to one month (Wang *et al.* 2013a) For each time point, 100 µl of the sample was collected, replaced with an equal volume of fresh PBS, and centrifuged at 12.000 rpm for 15 min. The supernatant was then collected and analysed using a Nanodrop at 260 nm to determine siRNA release. A cumulative siRNA release profile was created (Liu *et al.* 2012). All measurements were performed five times and the mean ± *SD* was recorded for each sample.

The *in vitro* stability study was conducted using the Eppendorf method at pH 5.0 and pH 7.4 under storage conditions of 4 and 25 °C for up to one month. For this, 1 mg/ml samples from each formulation were collected. The mean diameter and surface charge of particles were determined using DLS (Yadav *et al.* 2018).

2.6. Cell viability and apoptosis analysis

The apoptosis and necrosis behaviour of free siRNA, free CUR, TPU-Ole NPs, 100siRNA-TPU-Ole NPs, 600siRNA-TPU-Ole NPs, 100siRNA-2.5CUR-TPU-Ole NPs, 100siRNA-10CUR-TPU-Ole NPs, 600siRNA-2.5CUR-TPU-Ole

NPs, and 600siRNA-10CUR-TPU-Ole NPs on L929 and MCF-7 cells were evaluated in L929 and MCF-7 cells using the FITC-Annexin V/propidium iodide (PI) dual staining technique, followed by analysis with a FACS Calibur Flow Cytometer (BD Biosciences). MCF-7 and L929 cells were cultured in RPMI-1640 medium supplemented with 10% (v/v) FBS and 1% penicillin/streptomycin and seeded in T25 flasks at a density of 5×10^5 cells/mL in 5 ml of medium. The cells were then kept in an incubator at 37 °C with 5% CO_2 until reaching at least 80% confluence. Meanwhile, NPs (40 µg/mL) were incubated in 5 ml of nutrient medium overnight. Free siRNA and CUR were diluted to final concentrations of 30 µL/mL and 10 mg/mL. The following day, the medium in the flasks was replaced with 50% (v/v) extraction medium and incubated overnight. The next day, the cells were centrifuged at 4000 rpm for 5 min, washed three times with 1xPBS (pH 7.4), and resuspended in 500 µL of binding buffer according to the manufacturer's instructions. Staining was performed by adding 10 µL of staining solution (5 µL of Annexin V-FITC and 10 µL of PI), followed by incubation in the dark for 10 min, and immediately analysed using flow cytometry (Liu *et al.* 2012).

2.7. Cellular uptake of siRNA-TPU-Ole NPs and siRNA-CUR-TPU-Ole NPs

The cellular uptake of NPs was evaluated using confocal microscopy. FAM-labelled siRNA-NPs were used for this analysis. Cell nuclei were stained with 4′,6-diamidino-2-phenylindole (DAPI). Cells ($1x10^2$ cells/mL) were seeded on coverslips placed in a 24-well plate and allowed to adhere for 4 h in an incubator at 37 °C with 5% CO_2. 500 µL of extraction medium, prepared as described in the apoptosis analysis section, was added to the coverslips and incubated for 4 h. The cells were then fixed with 4% paraformaldehyde (PFA) solution, permeabilized with 0.2% Triton X-100, and stained with DAPI for 10 min. After staining, the cells were washed with 1xPBS (pH 7.4). The coverslips were visualised using a Zeiss LSM 800 Confocal Microscope (Jena, Germany) (Yang *et al.* 2011, Sun *et al.* 2018).

2.8. RT-PCR analysis

Comparative gene expression experiments were conducted using the Applied Biosystems QuantStudio 5 Real Time PCR system with five technical replicates. RNA isolation, cDNA synthesis, and the real-time PCR reaction were performed. L929 and MCF-7 cells were seeded at a concentration of 2.5×10^5 cells/well in 6 well plates and incubated for 24 h. After medium removal, the cells were treated with the experimental groups and incubated for an additional 24 h. RNA was extracted using lysis buffer for 1 min, following the manufacturer's protocol (Zymo Research, Quick RNA MiniPrep RNA Isolation Kit). The isolated RNAs were subjected to reverse transcription on ice using the High Capacity Reverse Transcription Kit (Applied Biosystems, Thermo Fisher Scientific). β-Actin was used as the reference gene. Gene expression analysis was conducted using the Viia7 Real-time PCR System (Thermo Fisher Scientific). All experiments were performed in five replicates, and cDNA without inclusions was used as the negative control group. Data was analysed using the Viia7 Real-Time PCR software (Yalcin *et al.* 2019).

RNA isolation was performed using the Zymo MiniPrep RNA kit. Cells were removed from the plate by adding 500 µl of lysis buffer. To activate the RNA isolation tubes, 100 µl of activation buffer was added and the tubes were centrifuged at 10000 g for 30 s. The lysate solutions, mixed with isopropanol were added to the activated RNA isolation tubes and centrifuged at 10000 g for 30 s. The isolated RNAs were washed with primary and secondary buffers. After removing the accumulated solution, it was centrifuged at 10000 g for 2 min to remove excess ethanol. The RNA isolation tubes were transferred to RNA/DNA-free tubes, 40 µl of elution buffer was added and incubated for 1 min. RNAs were accumulated in the tube by centrifugation at 10000 g for 1 min. The concentration of the obtained RNAs was measured using Nanodrop and the samples were diluted to ensure equal RNA concentrations across all groups. cDNA synthesis was performed using the Thermo Scientific Revert Aid First Strand cDNA kit. The reaction was carried out in a total volume of 20ul. The prepared reactions were incubated in a conventional PCR device under the recommended reaction conditions. The denaturation step was performed at 70 °C for 5 min, followed by cDNA synthesis at 50 °C for 60 min. The synthesised cDNAs were verified by electrophoresis before real-time PCR. The samples were analysed using the Comparative Ct method with five replicates per group. The ACTB gene was used as the reference gene. Results were analysed using the Applied Biosystems QuantStudio 5 device with QuantStudio Real Time PCR software Version 1.3. The primer sequences used in the study were as follows:

c-myc F: TGAGGAGACACCGCCCAC
c-myc R: CAACATCGATTTCTTCCTCATCTTC
ACTB F: AAGAGAGGCATCCTCACCCT
ACTB R: TACATGGCTGGGGTGTTGAA

2.9. Accuracy research

Under optimised conditions, accuracy research was conducted to ensure the reliability of analytical results from real samples. This research included evaluation of calibration equality, linearity, limit of detection (LOD), limit of measurement (LOQ), selectivity, matrix effect, accuracy survey, measurement uncertainty, precision, and accuracy. All accuracy studies were performed using calibration solution based on the solvent timeline.

2.10. Statistical analysis of results

All samples were studied in five replicates and the results were presented as mean ± standard deviation. GraphPad Prism program was used for statistical analysis and *p*-values <0.05 was considered statistically significant.

3. Results and discussion

3.1. The physicochemical characterisation of TPU-Ole polymers

3.1.1. GC-MS analysis

GC-MS is a mass scanning to determine the content and purity of an analyte. To determine the presence of isocyanate monomer residues in TPU-Ole, which could cause toxic effects, this analysis was performed. As shown in Figure 1(c), the TIC chromatograms of TPU and TPU-NPs at 10.125th min showed intense and less intense peaks, respectively, distinct from those of THF. Mass spectrum analysis of these peaks identified a spectrum consistent with diphenylmethane 4,4′-diisocyanate. Apart from this degradation product, no isocyanate residues were found in the sample. Thus, the synthesised product did not contain free isocyanate or isocyanate compounds bonded to non-monomer groups.

3.1.2. ^{1}HNMR analysis.

^{1}HNMR was used for the characterisation of the TPU-Ole (Figure 2(a)). The ether-methylene proton of the –COO–CH_2–CH_2–O– group in TPU was observed at 3.48 ppm. The CH_2 and C_6H_4 groups of TPU appeared at 1.2–1.3 and 7.3–8 ppm, respectively. The Ole displayed characteristic signals, including the hydrocarbon tail: –CH_3 at 0.85 ppm, –CH_2 at 1.5–2.4 ppm, –CH=CH– group at 5.3 ppm (small signal), m, –CH_2–CH_2–COOH group at 2.0 ppm, t, –CH_2–COOH at 2.3 ppm and –CH–OO– group at 3.5–4.1 ppm (Hazer *et al.* 2019).

3.1.3. GPC analysis

The molecular weight and molecular weight distribution of TPU-Ole were determined by GPC at 30 °C using THF as the eluent at a flow rate of 1 ml/min. As shown in Figure 2(b), TPU-Ole exhibited a unimodal homogeneous chain distribution. The molecular weight of the polymer was determined as 45 000 g/mol (Mn) and 108 000 g/mol (Mw), with a Mw/Mn ratio of 2.41. A narrow molecular weight distribution was observed based on the Mw/Mn ratio.

3.1.4. Thermal analysis

DSC analysis was conducted under nitrogen atmosphere at a flow rate of 50 ml/min. The polymer was heated from −50 to 190 °C. TGA was performed using a DSC/TGA Thermal Analysis System, where the polymer was heated from 20 to 600 °C at a rate of 10 °C/min. As shown from TGA curve (Figure 2(c)), the sample decomposed in three steps. The weight loss in the first step was attributed to the release of moisture and volatile substances. The degradation in the second step, occurring between 170 and 300 °C, was likely due to the breakdown of the bond between the Ole and the amino group. The degradation in the third step, occurring from 320 to 400 °C, corresponded to the degradation of the –CH_2OH– group. In TGA, the decomposition temperature of macroperoxide Ole in TPU-Ole polymer started at 350 °C, and the peak of the main degradation temperature was observed at around 400 °C. This decomposition temperature was associated with the bonding of TPU and Ole. Figure 2(d) showed the DSC cooling and heating curves of TPU-Ole, where the degradation started at about 159 °C and ended at 179 °C (Hazer *et al.* 2019, Amjed *et al.* 2022).

3.1.5. FTIR analysis

FTIR spectra of all samples were shown in Figure 3(a). The peaks corresponding to free and hydrogen bonded > C=O group presence in urethane linkage (–HN–CO…H–) of TPU were observed at around 1710 and 1700 cm^{-1}. The overlapping stretching vibrations of free and hydrogen bonded amine (–NH) groups in urethane and –OH stretching of Ole-COOH appeared at 3050–3750 cm^{-1} (Barick and Tripathy 2011). The stretching vibration of –N– group in TPU was observed at around 3323 cm^{-1}. The tensile band belonging to the –CH_2 group in urethane was seen at 2978 cm^{-1}. The skeletal vibration of C=C in the aromatic ring of urethane was detected at around 1597 cm^{-1} (Tang and Gao 2017). The characteristic peak of CUR was identified at around 2350 cm^{-1} in all CUR-NPs. Additionally, the phenolic O–H stretching vibration of CUR was found at around 3500 cm^{-1} (Anita *et al.* 2014). Due to the small amount of CUR loading, these peaks appeared with reduced intensity.

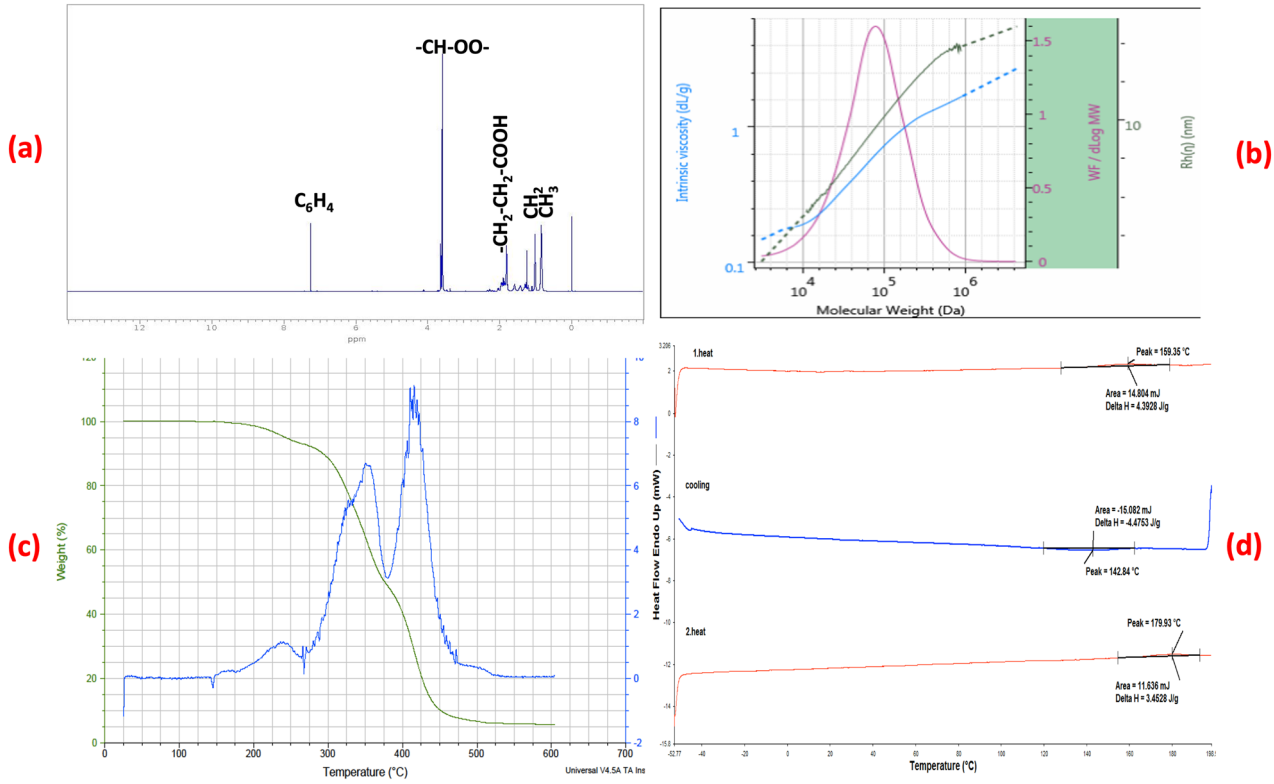

Figure 2. (a) ^{1}HNMR spectrum of TPU-Ole, showing the characteristic peaks at 7.3–8 ppm owing to C_6H_4 of TPU and 5.3 ppm owing to –CH = CH– of Ole were seen (b) GPC chromatogram of TPU-Ole. Mn and Mw were determined as 45 000 and 108 000 g/mol, respectively. (c) TGA curve of TPU-Ole, indicating that the degradation of oleic acid began at 350 °C with the main Td of oleic acid was observed at 400 °C and (d) DSC curve of TPU-Ole, showing thermal degradation starting at about 159 °C and ending at 179 °C.

3.1.6. XRD analysis

X-ray diffraction (XRD) analyses were performed using a Rigaku Ultima-IV X-ray diffractometer equipped with a copper target X-ray tube. Crystallographic information was provided by XRD for the structural characterisation of NPs. As shown in Figures 3(c,d), the XRD patterns of pure CUR, TPU-Ole NPs, 2.5CUR-TPU-Ole NPs, and 10CUR-TPU-Ole NPs were analysed. The samples were collected using an X-ray diffractometer at a 2θ diffraction angle and a rotating anode X-ray generator. Accordingly, characteristic peaks of pure CUR were observed at a series of 2θ diffraction angles: 7.94, 8.92, 12.02, 14.50, 15.68, 17.26, 18.06, 19.36, 21.1, 23.28, 23.68, 24.48, 25.48, 26.02, 26.66, 27.28, 28.08, and 29°. These data showed that pure CUR had a highly crystalline form (Donsi *et al.* 2010, Liu *et al.* 2022). However, the characteristic peaks of CUR were not observed in 2.5CUR-TPU-Ole NPs and 10CUR-TPU-Ole NPs, indicating that the CUR in NPs existed in an amorphous form.

Liu *et al.* prepared curcumin-loaded zein-tea saponin nanoparticles. XRD analysis was performed to detect the crystallinity of CUR in the composite NP. According to their results, the characteristic peaks of pure CUR at diffraction angles (2θ) of 8.90, 12.16, 14.51, 17.36, 23.44, and 25.55° indicated its crystalline form. The mixture of zein-TS-CUR and zein-CUR included similar diffraction angles showed that CUR was still in a crystalline state. However, the characteristic peaks belong to CUR were not found in CUR-NPs, meaning that CUR in CUR-NPs existed in an amorphous form (Liu *et al.* 2022).

3.2. Characterisation and morphology of NPs

The NP formulation was optimised by investigating the effects of polymer concentration (1, 3, and 5 mg/mL) and Tween 80 content (0.04, 0.08, and 0.02 ml/mL) and homogenisation speed (amplitude of 50, 70, and 90%) on the mean diameter distribution of particle using DLS. This evaluation identified the optimal parameters for achieving desirable NP characteristics. The mean diameter, polydispersity index (PDI), and ZP values of particles were analysed to determine the optimal formulation. Based on preliminary trials, the final optimised formulation was established, using 10 mg of TPU-Ole polymer. Tween 80 acting as a surfactant, reduced dynamic interfacial tension and stabilised the

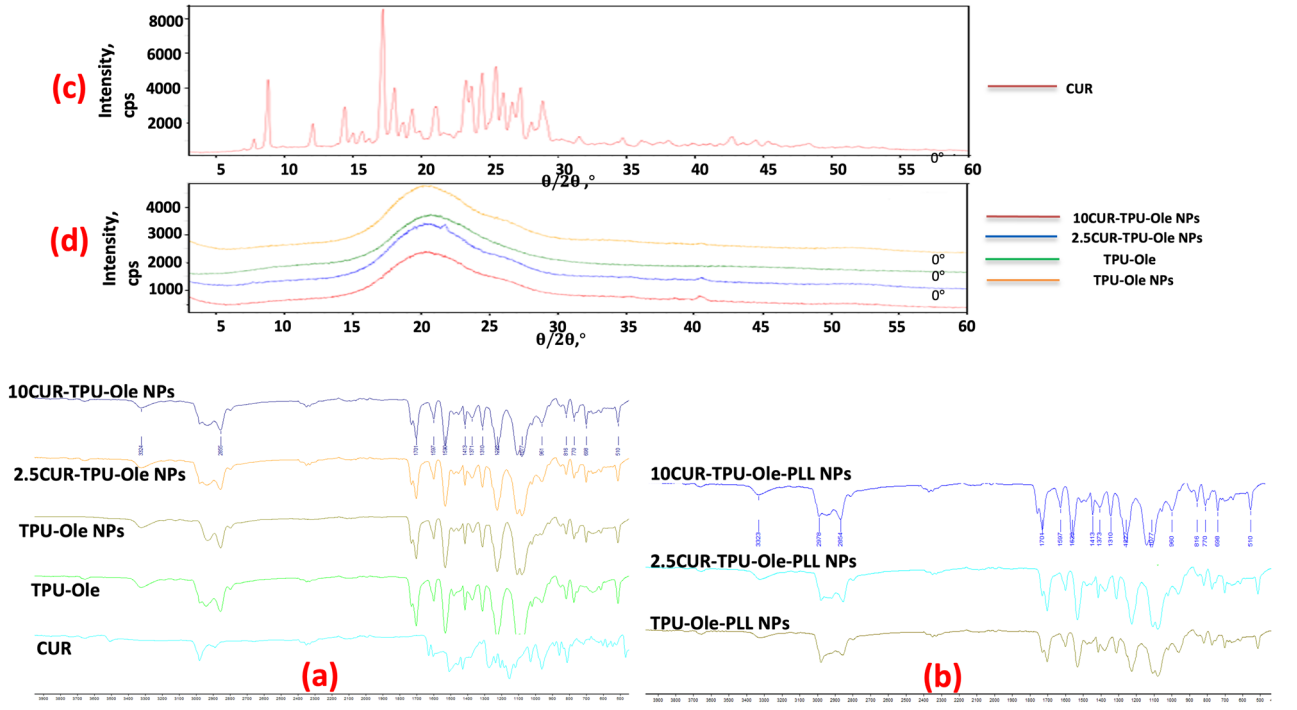

Figure 3. FTIR spectra of (a) CUR, TPU-Ole, TPU-Ole NPs, 2.5CUR-TPU-Ole NPs, 10CUR-TPU-Ole NPs; (b) TPU-Ole-PLL NPs, 2.5CUR-TPU-Ole-PLL NPs and 10CUR-TPU-Ole-PLL NPs. –N– and phenyl groups of TPU were observed at 3323 and 1597 cm^{-1}. –C=O group of Ole appeared at 1721 cm^{-1}. The characteristic peak of CUR was detected at ~2350 cm^{-1}; XRD patterns of (c) pure CUR, (d) TPU-Ole NPs, 2.5CUR-TPU-Ole NPs and 10CUR-TPU-Ole NPs. The characteristic diffraction peaks of pure CUR revealed at 7.94, 8.92, 12.02, 14.50, 15.68, 17.26, 18.06, 19.36, 21.1, 23.28, 23.68, 24.48, 25.48, 26.02, 26.66, 27.28, 28.08, and 29°. It was not observed for 2,5CUR-TPU-Ole NPs and 10CUR-TPU-Ole NPs, indicating amorphous state of CUR in NPs.

NPs by introducing an anionic component. The presence of Tween 80 enhanced steric repulsion among particles, leading to a decrease in mean diameter of particle. The incorporation of the drug into the NPs resulted in an increase in mean diameter due to the expansion of the polymeric matrix. A higher amount of polymer led to faster precipitation during the preparation process, contributing to larger mean diameter of particle. Homogenisation speed significantly influenced the mean diameter. Higher speeds resulted in smaller NPs as increased energy input into the suspension medium facilitated size reduction.

As a result of the optimisation studies, TPU-Ole NPs, 2.5CUR-TPU-Ole NPs, and 10CUR-TPU-Ole NPs were obtained with the mean diameters of 170 ± 2, 182 ± 4, and 189 ± 7 nm and PDI values of 0.011 ± 0.080, 0.135 ± 0.077, and 0.157 ± 0.018, respectively (Table 1(a)). The naked and CUR loaded formulations showed small mean diameter of particle which could be attributed to the well distribution of particles in dispersion medium. However, the mean diameter and polydispersity of CUR-NPs showed a slight increase as a result of drug encapsulation. The PDI values slightly increased in CUR loaded formulations. These values were within the acceptable range, indicating a narrow size distribution suitable for further *in vitro* studies. Surface charge analysis by ZP measurements showed values of −27.5 ± 0.11, −21.3 ± 0.33, and −19.8 ± 0.42 mV for TPU-Ole NPs, 2.5CUR-TPU-Ole NPs, and 10CUR-TPU-Ole NPs, respectively. The negative surface charge was attributed to the carboxyl group on the NP surface. A high ZP value provides a strong electrostatic repulsion that prevents particle aggregation, enhancing colloidal stability. The increase in the ZP of CUR NPs with increasing CUR content suggested that CUR was adsorbed onto the nanoparticle surface, masking the carboxyl groups and thereby reducing the negative ZP value. SEM and TEM images were taken to examine NP morphology. As shown in Figures 4(a–f), TPU-Ole NPs, 2.5CUR-TPU-Ole NPs, and 10CUR-TPU-Ole NPs appeared small, more spherical in shape and with a smooth surface.

3.3. Nanoparticles functionalised with PLL

The surfaces of all particles were modified by coating the NPs with PLL, which introduced a positive charge and enhanced the stability of the colloidal solution (Turino *et al.* 2021). The surface charges of PLL-NPs were determined by ZP measurements (Table 1(b))

Table 1. (a) Mean diameter, PDI, ZP, EE, and LE values of NPs; (b) the ZP values of cationic PLL-NPs showed a shift towards negative charges after interaction with negative charge of siRNA.

Samples, (a)	Mean diameter (nm)	PDI	ZP (mV)	EE (%, w/w)	LE (%, w/w)
TPU-Ole NPs	170 ± 2	0.011 ± 0.080	−27.5 ± 0.11	–	–
2.5CUR-TPU-Ole NPs	182 ± 4	0.135 ± 0.077	−21.3 ± 0.33	75 ± 0.12	14.2 ± 0.06
10CUR-TPU-Ole NPs	189 ± 7	0.157 ± 0.018	−19.8 ± 0.42	57 ± 0.23	28.8 ± 0.19
2.5CUR-TPU-Ole-100siRNA NPs	210 ± 2	0.023 ± 0.011	−10.6 ± 0.11	72 ± 0.09	13.7 ± 0.25
2.5CUR-TPU-Ole-600siRNA NPs	218 ± 2	0.065 ± 0.048	−13.82 ± 0.22	70 ± 0.31	12.5 ± 0.22
10CUR-TPU-Ole-100siRNA NPs	221 ± 3	0.008 ± 0.077	−9.1 ± 0.40	61.5 ± 0.16	25.3 ± 0.09
10CUR-TPU-Ole-600siRNA NPs	227 ± 4	0.020 ± 0.025	−12.02 ± 0.45	59 ± 0.20	23.6 ± 0.42

	ZP (mV)				
Samples, (b)	0 µl PLL	250 µl PLL	500 µl PLL	100 nM siRNA	600 nM siRNA
TPU-Ole NPs	−27.5 ± 0.11	+6.20 ± 0.24	+15.22 ± 0.19	−11.9 ± 0.08	−15.04 ± 0.34
2.5CUR-TPU-Ole NPs	−21.3 ± 0.33	+5.18 ± 0.09	+13.05 ± 0.44	−10.6 ± 0.11	−13.82 ± 0.22
10CUR-TPU-Ole NPs	−19.8 ± 0.42	+4.05 ± 0.61	+11.64 ± 0.78	−9.1 ± 0.40	−12.02 ± 0.45

ZP: zeta potential; TPU-Ole NPs: thermoplastic polyurethane-oleic acid nanoparticles; 2.5CUR-TPU-Ole NPs: 2.5 mg curcumin loaded thermoplastic polyurethane-oleic acid nanoparticles; 10CUR-TPU-Ole NPs: 10 mg curcumin loaded thermoplastic polyurethane-oleic acid nanoparticles; PLL: poly L lysine; TPU-Ole-PLL NPs: thermoplastic polyurethane-oleic acid-poly L lysine conjugated nanoparticles; 2.5CUR-TPU-Ole-PLL NPs: 2.5 mg curcumin loaded poly L lysine conjugated thermoplastic polyurethane-oleic acid nanoparticles; 10CUR-TPU-Ole-PLL NPs: 10 mg curcumin loaded poly L lysine conjugated thermoplastic polyurethane-oleic acid nanoparticles; 2.5CUR-TPU-Ole-100siRNA NPs: 2.5 mg curcumin loaded 100 nM siRNA conjugated thermoplastic polyurethane-oleic acid nanoparticles; 2.5CUR-TPU-Ole-600siRNA NPs: 2.5 mg curcumin loaded 600 nM siRNA conjugated thermoplastic polyurethane-oleic acid nanoparticles; 10CUR-TPU-Ole-100siRNA NPs: 10 mg curcumin loaded 100 nM siRNA conjugated thermoplastic polyurethane-oleic acid nanoparticles; 10CUR-TPU-Ole-600siRNA NPs: 10 mg curcumin loaded 600 nM siRNA conjugated thermoplastic polyurethane-oleic acid nanoparticles; EE: entrapment efficiency; LE: loading efficiency.

The optimised mean diameter of naked NPs was 170 ± 2 nm. CUR-NPs resulted in a slight increase in mean diameter. The negative ZP values were attributed to the presence of carboxyl groups on the NP surface, with a slight decrease in negativity observed upon CUR loading. As CUR concentration increased, drug LE increased whereas EE decreased, likely due to the increase tendency of CUR to aggregate and protrude from NPs; Results were expressed as mean ± *SD* ($n = 5$). Error bars represent *SD*, means $p < 0.05$.

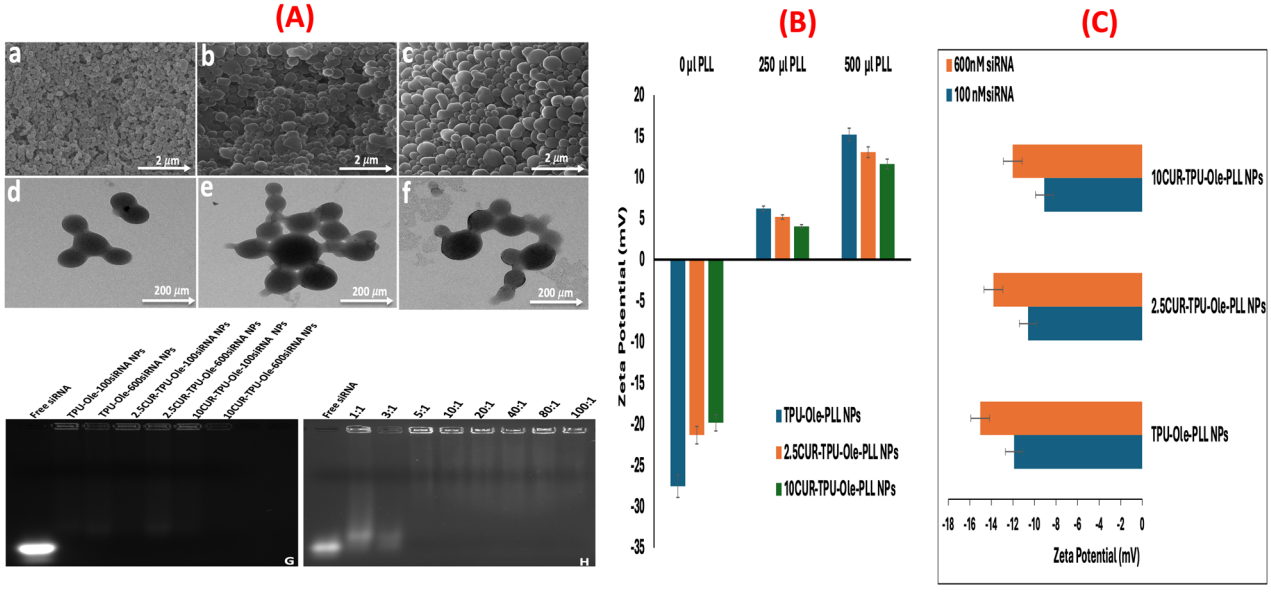

Figure 4. (A) SEM and TEM images of (a,d) naked TPU-Ole NPs, (b,e) 2.5CUR-TPU-Ole NPs, and (c,f) 10CUR-TPU-Ole NPs. Both SEM and TEM images confirmed that all NPs exhibited a spherical morphology with a smooth surface; agarose gel electrophoresis retention analysis of (g) free siRNA, TPU-Ole-100siRNA NPs, TPU-Ole-600siRNA NPs, 2.5CUR-TPU-Ole-100siRNA NPs, 2.5CUR-TPU-Ole-600siRNA NPs, 10CUR-TPU-Ole-100siRNA NPs, and 10CUR-TPU-Ole-600siRNA NPs. No visible siRNA band were detected, indicating strong complexation between NPs and siRNA, and (h) Free siRNA and NPs samples with different NPs/siRNA ratios. Faint siRNA bands were observed at N/P ratios of 1:1 and 3:1, corresponding to siRNA that had partially detached from the NPs; (B) ZP values of TPU-Ole NPs and CUR-TPU-Ole NPs after conjugation with 250 and 500 µl PLL. The surface charges of the NPs changed from negative to positive values due to PLL conjugation. These positive values were seen clearly, especially for 500 µl PLL concentration; (C) ZP values of siRNA-conjugated blank and CUR-loaded NPs at different concentrations; The ZP values of cationic PLL-NPs showed a shift towards negative charges after interaction with negative charge of siRNA. This effect was clearly seen especially at 600 nM siRNA. Results were expressed as mean ± SD (n = 5). Error bars represent SD, means $p < 0.05$. Abbreviations: PLL: poly L lysine; TPU-Ole-PLL NPs: thermoplastic polyurethane-oleic acid-poly L Lysine conjugated nanoparticles; 2.5CUR-TPU-Ole-PLL NPs: 2.5 mg curcumin loaded poly L Lysine conjugated thermoplastic polyurethane-oleic acid nanoparticles; 10CUR-TPU-Ole-PLL NPs: 10 mg curcumin loaded poly L Lysine conjugated thermoplastic polyurethane-oleic acid nanoparticles.

and these values were found to be +6.20 ± 0.24; +5.18 ± 0.09; +4.05 ± 0.61 mV for TPU-Ole-250 µl PLL NPs; 2.5CUR-TPU-Ole-250 µl PLL NPs; 10CUR-TPU-Ole-250 µl PLL NPs and +15.22 ± 0.19; +13.05 ± 0.44; +11.64 ± 0.78 for TPU-Ole-500 µl PLL NPs; 2.5CUR-TPU-Ole-500 µl PLL NPs; 10CUR-TPU-Ole-500 µl PLL NPs respectively (Figure 4(b)). The surface charges of the NPs shifted from negative to positive depending on the PLL concentration. The amount of PLL used was limited, as excessive addition of PLL could have a toxic effect on cells. In the conjugation reaction, the highest ZP values and stability were obtained with 500 µl of PLL and therefore, this concentration was used in the subsequent steps. The FTIR spectra of empty and CUR-NPs modified with PLL are shown in Figure 3(b). Due to the low PLL concentration, its characteristic peaks were not distinctly observed in the spectrum.

3.4. The conjugation of cmyc siRNA with TPU-Ole-PLL NPs and CUR-TPU-ole NPs

The conjugation reaction occurred due to the electrostatic interaction between positively charged PLL-NPs and negatively charged c-myc siRNA (Meyer *et al.* 2009, Liu *et al.* 2012). In this process, PLL played a crucial role in stabilising siRNA binding, enhancing electrostatic attraction, and preventing repulsion. The polycationic nature of PLL facilitated the assembly of oppositely charged molecules onto the NP surface, improving conjugation efficiency. This functionalization step further enhanced cellular uptake, siRNA transfection efficiency, and controlled gene silencing, supporting its application in targeted cancer therapy (Gorzkiewicz *et al.* 2020).

DLS analysis revealed that after interaction with siRNA (Table 1(b)), the positive surface charges of all NPs shifted to negative values (Figure 4(c)). This change confirmed the successful binding of c-myc siRNA to NPs. The negatively charged phosphate groups of siRNA neutralised the positive charges of PLL-NPs, leading to a reduction in the positive charges of NPs (Raja *et al.* 2015). This effect was particularly evident upon binding of 600 nM siRNA to the naked NP, which had a ZP value of −15.04 ± 0.34 mV. According to DLS analysis, these results illustrated the successful association of siRNA with NP.

After conjugation with siRNA, the binding efficiencies of TPU-Ole-100siRNA NPs, TPU-Ole-600siRNA NPs, 2.5CUR-TPU-Ole-100siRNA NPs, 2.5CUR-TPU-Ole-600siRNA NPs, 10CUR-TPU-Ole-100siRNA NPs, and 10CUR-TPU-Ole-600siRNA were 85 ± 0.17, 89 ± 0.33, 77 ± 0.09, 80 ± 0.13, 79 ± 0.24, and 91 ± 0.05% w/w, respectively. These differences in binding efficiency were attributed to the negative ZP values on the NPs, which influenced electrostatic interactions with siRNA.

3.5. Encapsulation efficiency of CUR

As seen in Table 1(a), the EE and LE of 2.5CUR-TPU-Ole NPs, 10CUR-TPU-Ole NPs, 2.5CUR-TPU-Ole-100siRNA NPs, 2.5CUR-TPU-Ole-600siRNA NPs, 10CUR-TPU-Ole-100siRNA NPs, and 10CUR-TPU-Ole-600siRNA NPs were 75 ± 0.12, 57 ± 0.23, 72 ± 0.09, 70 ± 0.31, 61.5 ± 0.16, 59 ± 0.20% w/w for EE and 14.2 ± 0.06, 28.8 ± 0.19, 13.7 ± 0.25, 12.5 ± 0.22, 25.3 ± 0.09, 23.6 ± 0.42% w/w for LE, respectively. Higher drug loading resulted in lower EE. As the CUR concentration increased, the tendency of the NPs to protrude CUR also increased (Meng *et al.* 2021), which was consistent with the findings of Sarpoli *et al.* It was reported that increasing CUR concentration could lead to decrease in EE due to the saturation of the NP's loading capacity (Sarpoli *et al.* 2022). The LE of siRNA-CUR-TPU-Ole NPs was slightly lower than that of CUR-TPU-Ole NPs. This reduction was due to the release of CUR adsorbed on NPs surface during the siRNA binding process (Anitha *et al.* 2014). Nevertheless, CUR, due to its hydrophobic nature, was effectively loaded into the core of the hydrophobic TPU-Ole NPs (Meng *et al.* 2021). In conclusion, our findings highlighted the importance of optimising loading conditions for multiple therapeutic agents to maximise clinical efficacy.

In a study by Woo *et al.*, stearic acid-oleic acid nanoparticles (SONs) with a high loading of salicylic acid were developed. To optimise encapsulation efficiency, salicylic acid loaded SONs were prepared with varying ratios of oleic acid (OA). *In vitro* release study was also conducted. The encapsulation efficiency enhanced from 49 to 69% as the OA ratio increased from 0 to 40 wt %. The incorporation of OA into the solid lipid matrix increased the amorphous proportion, reducing particle crystallinity and increasing encapsulation capacity. The crystallinity degree of lipid NPs correlated with encapsulation efficiency. The disruption of the crystalline matrix by OA created additional space for salicylic acid loading, thereby enhancing encapsulation efficiency. Based on these findings, SONs containing 30 wt % OA were selected for *in vitro* release study. The initial fast release was observed due to the diffusion of free salicylic acid through the membrane. The second phase showed a much slower release rate due to the retention of salicylic acid in the SON particle dispersion. The controlled release behaviour proved the successful incorporation of salicylic acid in the SON matrix (Woo *et al.* 2014).

3.6. Stability study of NPs based on TPU-ole

All samples were stored at pH 5.0 and 7.4, at 4 and 25 °C for one month and their mean diameter, PDI, and ZP values were observed during this time. Since aggregation and instability of the NPs were observed within the first week at 25 °C, the stability study was conducted at 4 °C. As shown in Table 2, the amine group of PLL was exposed to protonation at the acidic pH 5.0 of the endosome and lysosome in tumour cells, leading to the NP expansion and swelling due to the charge repulsion effect known as the proton sponge effect. Additionally, the hydrophilic nature of PLL, compared to the hydrophobic TPU-Ole, facilitated the entry of water into the NPs. This process resulted in NP expansion in the acidic environment due to osmotic pressure and electrostatic repulsion. The osmotic pressure arose from the concentration gradient between the particle interior and the surrounding aqueous medium. However, the hydrophilic-hydrophobic balance maintained structural integrity by preventing excessive swelling.

Table 2 shows the changes in the mean diameter, PDI, and ZP values of NPs at pH 5.0 and 4 °C over a 30-day period. The particle mean diameter of TPU-Ole NPs, 2.5CUR-TPU-Ole NPs, 10CUR-TPU-Ole NPs, TPU-Ole-100siRNA NPs, TPU-Ole-600siRNA NPs, 2.5CUR-TPU-Ole-100siRNA NPs, 2.5CUR-TPU-Ole-600siRNA NPs, 10CUR-TPU-Ole-100siRNA NPs, 10CUR-TPU-Ole-600siRNA NPs were about 170 ± 2, 182 ± 4, 189 ± 7, 192 ± 5, 198 ± 6, 210 ± 2, 218 ± 2, 221 ± 3, and 227 ± 4 nm, respectively for the first day. By the end of the month, these values increased to 185 ± 7, 193 ± 5, 197 ± 5, 240 ± 3, 261 ± 4, 268 ± 8, 297 ± 9, 300 ± 7, and 335 ± 2 nm, respectively. All samples exhibited a narrow size distribution on the first day, while this effect slightly reduced by the end of one month. A moderate increase in particle mean diameter was observed by day 30. A slight aggregation was seen at the end of day 30, along with an increase in mean diameter and PDI values compared to the first day. Initially, both empty and CUR-NPs had a negative ZP value. However, modification with PLL resulted in a shift towards positive ZP value. Following siRNA conjugation, the surface charges of all samples became negative. Upon exposure to pH 5.0, the protonation of PLL's amine group induced a cationic polyelectrolyte effect. As the electrostatic interactions between PLL NPs with siRNA weakened, a neutralisation effect emerged, reducing the magnitude of the negative surface charge. Despite these changes, the mean particle diameter and PDI remained relatively stable across different pH conditions, confirming the overall stability of NPs in PBS.

Table 2. Changes in mean diameter, PDI, ZP, EE%, and LE% of TPU-Ole-based NPs after 30 days of storage at pH 5.0 and 7.4 (4 °C).

Samples	Time	Mean diameter (nm) (pH 5.0)	PDI (pH 5.0)	ZP (mV) (pH 5.0)	EE%-LE% (w/w) (pH 5.0)	Mean diameter (nm) (pH 7.4)	PDI (pH 7.4)	ZP (mV) (pH 7.4)	EE%-LE% (w/w) (pH 7.4)
TPU-Ole NPs	Day 1	170 ± 2	0.011 ± 0.080	−27.5 ± 0.11	–	170 ± 2	0.011 ± 0.080	−27.5 ± 0.11	–
	Day 30	185 ± 7	0.076 ± 0.098	−20.9 ± 0.13		179 ± 1	0.077 ± 0.010	−20.2 ± 0.07	
2.5CUR-TPU-Ole NPs	Day 1	182 ± 4	0.135 ± 0.077	−21.3 ± 0.33	75 ± 0.12–14.2 ± 0.06	182 ± 4	0.135 ± 0.077	−21.3 ± 0.33	75 ± 0.12–14.2 ± 0.06
	Day30	193 ± 5	0.093 ± 0.046	−16.8 ± 0.45	63 ± 0.12–12.3 ± 0.12	190 ± 3	0.090 ± 0.89	−17.7 ± 0.45	66 ± 0.14–12.9 ± 0.18
10CUR-TPU-Ole NPs	Day 1	189 ± 7	0.157 ± 0.018	−19.8 ± 0.42	57 ± 0.23–28.8 ± 0.19	189 ± 7	0.157 ± 0.018	−19.8 ± 0.42	57 ± 0.23–28.8 ± 0.19
	Day 30	197 ± 5	0.169 ± 0.111	−11.9 ± 0.50	51 ± 0.22–25.3 ± 0.19	194 ± 2	0.169 ± 0.023	−14.5 ± 0.05	53 ± 0.11–24.9 ± 0.20
TPU-Ole-100siRNA NPs	Day 1	192 ± 5	0.034 ± 0.045	−11.9 ± 0.08	–	192 ± 5	0.034 ± 0.045	−11.9 ± 0.08	–
	Day 30	240 ± 3	0.290 ± 0.056	−4.3 ± 0.02		205 ± 4	0.028 ± 0.024	−9.7 ± 0.13	
TPU-Ole-600siRNA NPs	Day 1	198 ± 6	0.081 ± 0.033	−15.04 ± 0.34	–	198 ± 6	0.081 ± 0.033	−15.04 ± 0.34	–
	Day 30	261 ± 4	0.140 ± 0.019	−7.6 ± 0.14		212 ± 4	0.102 ± 0.067	−13.8 ± 0.07	
2.5CUR-TPU-Ole-100siRNA NPs	Day 1	210 ± 2	0.023 ± 0.011	−10.6 ± 0.11	72 ± 0.09–13.7 ± 0.25	210 ± 2	0.023 ± 0.011	−10.6 ± 0.11	72 ± 0.09–13.7 ± 0.25
	Day 30	268 ± 8	0.099 ± 0.078	−4.4 ± 0.32	57 ± 0.13–11.8 ± 0.11	219 ± 6	0.127 ± 0.043	−9.5 ± 0.72	60 ± 0.17–11.3 ± 0.18
2.5CUR-TPU-Ole 600siRNA NPs	Day 1	218 ± 2	0.065 ± 0.048	−13.82 ± 0.22	70 ± 0.31–12.5 ± 0.22	218 ± 2	0.065 ± 0.048	−13.82 ± 0.22	70 ± 0.31–12.5 ± 0.22
	Day 30	297 ± 9	0.319 ± 0.066	−6.7 ± 0.09	55 ± 0.15–10.6 ± 0.17	222 ± 1	0.088 ± 0.011	−12.1 ± 0.41	62 ± 0.13–11.24 ± 0.19
10CUR-TPU-Ole-100siRNA NPs	Day 1	221 ± 3	0.008 ± 0.077	−9.1 ± 0.40	61.5 ± 0.16–25.3 ± 0.09	221 ± 3	0.008 ± 0.077	−9.1 ± 0.40	61.5 ± 0.16–25.3 ± 0.09
	Day 30	300 ± 7	0.087 ± 0.052	−5.9 ± 0.06	46 ± 0.11–22.2 ± 0.15	250 ± 5	0.109 ± 0.089	−7.9 ± 0.18	50 ± 0.02–21.6 ± 0.15
10CUR-TPU-Ole-600siRNA NPs	Day 1	227 ± 4	0.020 ± 0.025	−12.02 ± 0.45	59 ± 0.20–23.6 ± 0.42	227 ± 4	0.020 ± 0.025	−12.02 ± 0.45	59 ± 0.20–23.6 ± 0.42
	Day 30	335 ± 2	0.311 ± 0.032	−4.1 ± 0.58	44 ± 0.13–22.5± 0.22	261 ± 8	0.132 ± 0.033	−11.7 ± 0.06	46 ± 0.10–21.0 ± 0.14

A slight increase in mean diameter and PDI with a reduction in negative ZP values was observed, more pronounced at acidic pH. siRNA conjugation shifted towards less negative values of ZP. All formulations retained structural stability. EE% and LE% values indicated sustained drug retention within the NPs over 30 days Data are presented as mean ± *SD* ($n = 5$); $p < 0.05$ was considered significant.

Table 2 shows the changes in mean diameter, PDI, and ZP values of the samples at pH 7.4 and 4 °C over a 30-day period. On the first day, the mean diameter of TPU-Ole NPs, 2.5CUR-TPU-Ole NPs, 10CUR-TPU-Ole NPs, TPU-Ole-100siRNA NPs, TPU-Ole-600siRNA NPs, 2.5CUR-TPU-Ole-100siRNA NPs, 2.5CUR-TPU-Ole-600siRNA NPs, 10CUR-TPU-Ole-100siRNA NPs, 10CUR-TPU-Ole-600siRNA NPs were about 170 ± 2, 182 ± 4, 189 ± 7, 192 ± 5, 198 ± 6, 210 ± 2, 218 ± 2, 221 ± 3, and 227 ± 4 nm, respectively. By the end of the month, these values changed to 179 ± 1, 190 ± 3, 194 ± 2, 205 ± 4, 212 ± 4, 219 ± 6, 222 ± 1, 250 ± 5, and 261 ± 8 nm, respectively. The NPs remained stable over 30 days, maintaining a narrow size distribution. Excessive swelling was prevented by the deprotonation of PLL's amine group in the alkaline environment. Consequently, only a slight increase in particle mean diameter was observed at the end of the month. According to the short-term stability study, the largest mean diameter of particle was 335 nm, while all other values remained within an ideal range. Overall, all NP formulations exhibited high stability and resistance to aggregation in buffer solutions at both pH 5.0 and 7.4 over the 30-day period.

Maintaining NP stability at physiological pH (7.4) and 4 °C is crucial for preserving their structural integrity and ensuring consistent therapeutic efficacy during circulation and storage. In contrast, the reduced stability observed at pH 5.0, which mimics the acidic tumour microenvironment and intracellular compartments, such as endosomes and lysosomes, facilitated the controlled release of encapsulated agents like CUR and siRNA. This pH-responsive behaviour is advantageous for targeted cancer therapy, as it enables site-specific drug release while minimising systemic side effects. For instance, Tang *et al.* developed pH-sensitive poly(β-amino ester) nanoparticles co-delivering siRNA and paclitaxel, which demonstrated enhanced anticancer efficacy in breast cancer models. Their stability at physiological pH and controlled release in acidic environments contributed to improve therapeutic outcomes (Tang *et al*. 2015).

Ma *et al.* prepared siRNA-conjugated polydimethylaminoethyl methacrylate and poly(oligo(ethylene glycol) methyl ether methacrylate) (PDMAEMA-POEGMA) star NPs to suppress βIII-tubulin and Polo-Like Kinase 1 (PLK1) genes for lung cancer treatment. The positively charged polyelectrolyte PDMAEMA was conjugated with anionic siRNA. The resulting star NPs exhibited a mean diameter of 14.4 nm, a PDI of 0.18, and a positive surface charge of 8.5 mV at neutral pH. An increase in surface charge was observed under acidic pH. The surface charge enhanced 2.5-fold at pH 6 (+21.5 mV) and 3.2-fold at pH 5 (+26.8 mV). As a result, NPs were pH sensitive under acidic environment, such as the endosome (pH 6) and lysosome (pH 5). Similar increases in surface charge were observed after siRNA binding with NPs (Ma *et al.* 2022).

3.7. In vitro release study

The *in vitro* CUR release from all NPs was evaluated in PBS under both physiological (pH 7.4) and acidic tumor-representative environment (pH 5.0). Figures 5(a,b) showed *in vitro* release profiles of CUR from 2.5CUR-TPU-Ole NPs and 10CUR-TPU-Ole NPs at both pH 5.0 and pH 7.4. In Figure 5(a), as a result of the initial burst effect at pH 5.0, about 9% w/w of CUR released from 2.5CUR-TPU-Ole NPs within the first 12 h and 4.6% w/w from 10CUR-TPU-Ole NPs within the first 7 h, followed by a sustained release phase. The release reached a plateau after 672 h, with 78% w/w of CUR released from 2.5CUR-TPU-Ole NPs and 63% w/w from 10CUR-TPU-Ole NPs.

At pH 7.4 (Figure 5(b)), the burst release effect resulted in the release of 8.6% w/w CUR from 2.5CUR-TPU-Ole NPs within the first 10 h and 5.6% w/w from 10CUR-TPU-Ole NPs within the first 12 h. The release gradually continued, reaching a plateau by the 26th day, with 64.7% w/w of CUR released from 2.5CUR-TPU-Ole NPs within 648 h and 55% w/w from 10CUR-TPU-Ole NPs within 672 h.

Figure 5(c) showed the *in vitro* release profile of siRNA from siRNA-NPs. At pH 5.0, an initial burst release was around 11.20% w/w for 2.5CUR-TPU-Ole-100siRNA NPs in the first 4 h; 11.20% w/w for 2.5CUR-TPU-Ole-600siRNA NPs at 7h; 13.40% w/w for 10CUR-TPU-Ole-100siRNA NPs at 4.5 h; 11.70% w/w for 10CUR-TPU-Ole-600siRNA NPs at 4.5 h; 19% w/w for TPU-Ole-100siRNA NPs at 10 h and 13% w/w for TPU-Ole-600siRNA at 12 h, followed by an extended release phase. By the end of the 27th day, siRNA release reached a plateau with a release rate of 61.6% w/w from TPU-Ole-100siRNA NPs within 672 h; 57.80% w/w from TPU-Ole-600siRNA NPs within 648 h; 82.50% w/w from 10CUR-TPU-Ole-600siRNA NPs within 672 h; 88.10% w/w from 10CUR-TPU-Ole-100siRNA NPs within 648 h; 93.55% w/w from 2.5CUR-TPU-Ole-600siRNA NPs within 672 h and 96.90% w/w from 2.5CUR-TPU-Ole-100siRNA NPs within 672 h.

In Figure 5(d), the initial burst effect of siRNA at pH 7.4 was about 17.3% w/w for 2.5CUR-TPU-Ole-100siRNA NPs at 12 h; 14.6% w/w for 2.5CUR-TPU-Ole-600siRNA NPs at 12h; 13.8% w/w for 10CUR-TPU-Ole-100siRNA NPs at 12h; 11.6% w/w for 10CUR-TPU-Ole-600siRNA NPs at 12h; 11.3% w/w for TPU-Ole-100siRNA NPs at 12 h and 7.4% w/w for TPU-Ole-600siRNA NPs at 12 h, followed by a slower and continuous extended release. By the end of

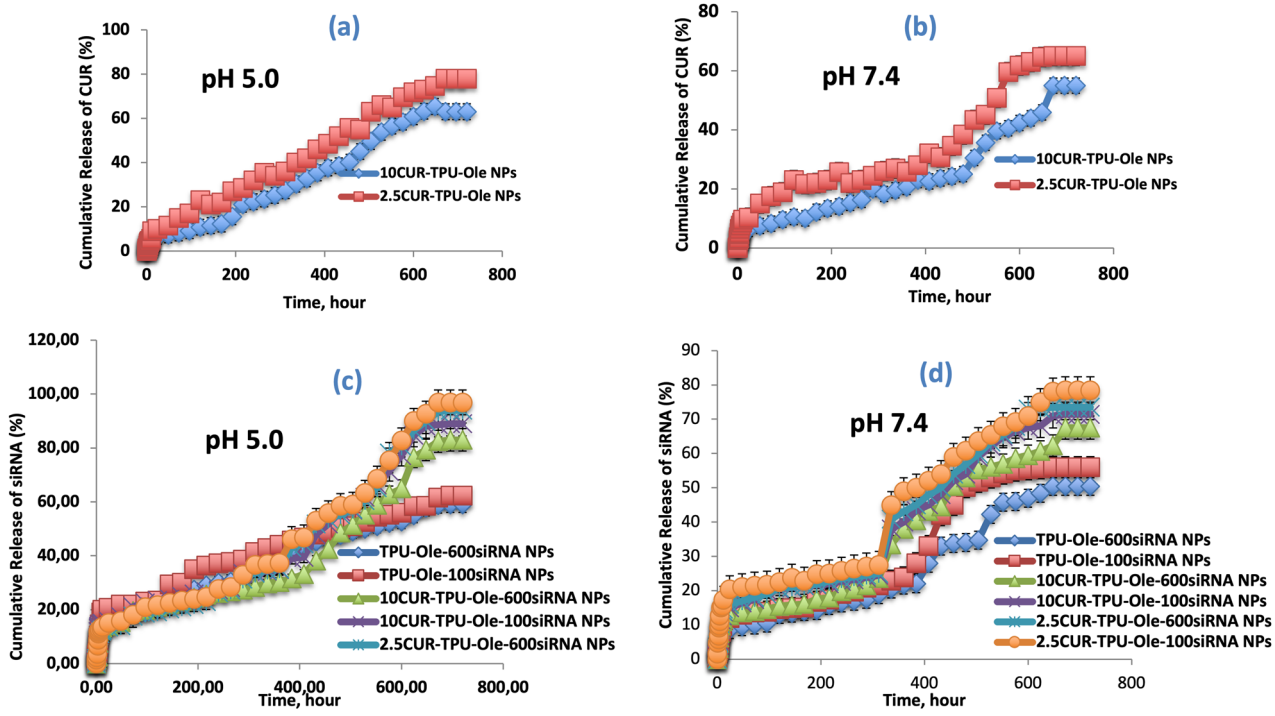

Figure 5. *In vitro* release profiles of CUR and siRNA from different NP formulations under pH 5.0 and pH 7.4 conditions. (a) CUR released at pH 5.0: 78 ± 1.7 and 63 ± 0.6% of CUR were released from 2.5CUR-TPU-Ole NPs and 10CUR-TPU-Ole NPs, (b) CUR released at pH 7.4: 64.7 ± 1.1 and 55 ± 2.5% of CUR were released from 2.5CUR-TPU-Ole NPs and 10CUR-TPU-Ole NPs, (c) siRNA released at pH 5.0: 61.6 ± 2.8, 57.8 ± 1.5, 82.5 ± 1.8, 88.1 ± 0.9, 93.55 ± 2.4, and 96.9 ± 0.2% of siRNA were released from TPU-Ole-100siRNA NPs, TPU-Ole-600siRNA NPs, 10CUR-TPU-Ole-600siRNA NPs, 10CUR-TPU-Ole-100siRNA NPs, 2.5CUR-TPU-Ole-600siRNA NPs, and 2.5CUR-TPU-Ole-100siRNA NPs, (d) siRNA released at pH 7.4: 55.7 ± 0.1, 50.4 ± 0.6, 67.5 ± 0.3, 71 ± 1.7, 72.9 ± 2.8, and 75 ± 0.9% of siRNA were released from TPU-Ole-100siRNA NPs, TPU-Ole-600siRNA NPs, 10CUR-TPU-Ole-600siRNA NPs, 10CUR-TPU-Ole-100siRNA NPs, 2.5CUR-TPU-Ole-600siRNA NPs, and 2.5CUR-TPU-Ole-100siRNA NPs. Error bars represented the standard deviation of five independent measurements ($n = 5$, $p = 0.001$, $p < 0.05$).

about the 25th day, siRNA release reached a plateau with a release rate of 55.7% w/w from TPU-Ole-100siRNA NPs within 624 h; 50.4% w/w from TPU-Ole-600siRNA NPs within 648 h; 67.5% w/w from 10CUR-TPU-Ole-600siRNA NPs within 672 h; 71% w/w from 10CUR-TPU-Ole-100siRNA NPs within 648 h; 72.9% w/w from 2.5CUR-TPU-Ole-600siRNA NPs within 600 h and 75% w/w from 2.5CUR-TPU-Ole-100siRNA NPs within 624 h.

According to the results, the initial burst release occurred at both pH 5 and 7.4 due to the loss of superficial CUR adsorbed on the hydrophilic regions. The slower and continuous release could be attributed to the diffusion of CUR from the hydrophobic core of the particle. The cumulative release of siRNA and CUR from NPs was higher at pH 5 compared to pH 7.4. In particular, the siRNA release rate was higher than that of CUR. The hydrophobic and hydrophilic properties of the encapsulated CUR and siRNA effected the release profile. Due to the hydrophilic nature of siRNA, it acts as a water channel, increasing water transfer to the hydrophobic core of the NP. This effect reduced the stability of the particle to a certain extent and allowed CUR and siRNA to be released more quickly. Therefore, siRNA release from CUR-siRNA NPs at pH 5 and pH 7.4 was observed at a higher rate than from siRNA-NPs. These results indicated that the release of the therapeutic agents from NPs was pH-dependent. CUR and siRNA release were higher at acidic pH 5 compared to pH 7.4. PLL was easily protonated at low pH and lowering the pH also leaded to the protonation of CUR, which reduced the retention capacity of CUR in the NP and facilitated the release of the chemical agent into the acidic environment. Additionally, CUR release was relatively slow compared to siRNA. This could be attributed to the high stability of the core-shell structure of TPU-Ole NPs (Lin *et al.* 2014). Clinically, the initial burst release observed in this study was needed to achieve a high concentration of the agent in the target tissue. As a result, TPU-Ole NPs demonstrated promising carrier for loading and delivering poorly water soluble agents in a controlled manner.

The pH-responsive behaviour of these NPs is particularly advantageous for clinical applications in cancer therapy. The acidic microenvironment of tumour tissues (pH ~6.5) and intracellular compartments, such as endosomes and lysosomes (pH 5.0–5.5) can trigger the

release of therapeutic agents from pH-sensitive nanocarriers. This targeted release mechanism enhances the therapeutic efficacy of the encapsulated agents while minimising systemic side effects. For instance, Zhang *et al.* designed PEG-DOX-Cur nanoparticles for the co-delivery of Cur and DOX, demonstrating enhanced anticancer efficacy due to the selective release of the drugs in the acidic tumour microenvironment (Zhang *et al.* 2016). Similarly, Gao *et al.* developed pH-responsive prodrug nanoparticles based on a sodium alginate derivative for the co-release of doxorubicin and curcumin into tumour cells, achieving improved therapeutic outcomes (Gao *et al*. 2017). These studies highlighted the potential of pH-sensitive nanocarriers in enhancing the therapeutic efficacy of co-delivered anticancer agents by exploiting the acidic tumour microenvironment.

In another study, Ghaffari *et al.* designed PAMAM-Cur/Bcl-2 siRNA polyplex NPs by grafting Bcl-2 siRNA to the curcumin (Cur) loaded polyamidoamine (PAMAM) dendrimer structure to achieve the simultaneous release of Cur and SiRNA. The *in vitro* release profile was evaluated at pH 5.4 and 7.4. About 40% of Cur was released within 72 h at pH 5.4 and 10% at pH 7.4, followed by sustained release (Ghaffari *et al.* 2020).

3.8. Evaluation of complexing property by agarose gel electrophoresis

The ability of cationic PLL-TPU-Ole NPs to bind anionic siRNA is a crucial parameter in gene delivery. Agarose gel electrophoresis was performed to evaluate the binding affinity of cationic TPU-Ole NPs to anionic siRNA. Different ratios of NPs/siRNA (N/P) (1:1, 3:1, 5:1, 10:1, 20:1, 40:1, 80:1, 100:1) were prepared and all images were created in agarose gel electrophoresis to determine the optimal NPs/siRNA ratio and maximum siRNA complexation. In Figure 4(g), a band of free siRNA was observed. In contrast, no band was detected in electrophoresis for TPU-Ole-100siRNA NPs, TPU-Ole-600siRNA NPs, 2.5CUR-TPU-Ole-100siRNA NPs, 2.5CUR-TPU-Ole-600siRNA NPs, 10CUR-TPU-Ole-100siRNA NPs, and 10CUR-TPU-Ole-600siRNA NPs due to the strong complexation of NPs with siRNA. In Figure 4(h), a faint band of free siRNA was seen at N/P ratios of 1:1 and 3:1. As the number of amino groups in PLL-functionalised TPU-Ole NPs increased with an NPs/siRNA ratio of 5/1 and above, siRNA migration was completely delayed, resulting in the disappearance of the trace. This finding suggested an enhanced ability of these groups to condense siRNA onto NP surface (Lin *et al.* 2014). It was concluded that the polyplexes had a high potential to complex with siRNA.

Shirangi *et al.* prepared superparamagnetic iron oxide nanoparticles decorated with silk sericin (SS NPs) for the targeted delivery of ROR1 siRNA to silence human ROR1 gene expression. They tested the binding efficiency of siRNA to cationic SSP NPs using the agarose gel electrophoresis. Compared to the control group siRNA, no band of siRNA was observed in the siRNA-bound samples at all ratios, except for a band of free siRNA. Further increasing the number of NPs did not additionally affect the retention of siRNA molecules (Shirangi *et al.* 2022).

Clinically, the efficient complexation of siRNA with NPs is paramount for successful gene silencing therapies. Stable NP-siRNA complexes protect siRNA from enzymatic degradation, facilitate cellular uptake, and ensure effective release within target cells. The use of agarose gel electrophoresis to confirm complete siRNA binding at optimal N/P ratios is essential in the development of gene delivery systems, as it directly correlates with the therapeutic potential of siRNA-based interventions. For instance, Eljack *et al.* demonstrated that their targeted stealth magnetic siRNA nanovectors (TS-MSN) effectively complexed siRNA without leakage, as evidenced by agarose gel electrophoresis, leading to significant gene knockdown in HER2+ breast cancer cells (Eljack *et al.* 2022).

3.9. Cell viability and apoptosis analysis

The behaviour of NPs on MCF-7 and L929 cells was examined using flow cytometry, and the distribution of apoptotic, necrotic, and viable cell percentages was presented in Table 3. Due to the higher siRNA binding efficiency, NP formulations conjugated with 600 nM siRNA were selected and used. The graph for each group was shown in Figure 6. Q1, Q2, Q3, and Q4 corresponded to necrotic, late apoptotic, viable, and early apoptotic cells, respectively. Cell viability in L929 cells after interaction with NPs was slightly higher than in MCF-7 cells. For instance, treatment with 10CUR-600siRNA resulted in 62.9% viable cells in L929 cells compared to 49.7% in MCF-7 cells. Within the L929 cell group, siRNA-NPs exhibited the lower cytotoxicity, with a viability rate of 70.2%. Meanwhile, formulations containing CUR, siRNA, 2.5CUR-TPU-Ole-600siRNA NPs, and 10CUR-TPU-Ole-600siRNA NPs displayed similar viability percentages. The relatively lower cell viability observed in L929 cells compared to MCF-7 cells could be attributed to the siRNA concentration used. The observed differential cytotoxicity of siRNA-NPs on MCF-7 and L929 cells underscored the potential of siRNA-based therapies in cancer treatment. The higher binding affinity and subsequent gene silencing in

Table 3. Cell apoptosis and necrosis rates identified by flow cytometry.

Samples	Q1 (%)	Q2 (%)	Q3 (%)	Q4 (%)
Control MCF-7	2.5	0.1	77.1	1.6
CUR	1.6	1.0	60.1	2.3
siRNA	2.2	1.4	60.3	8.4
TPU-Ole-600siRNA NPs	20.2	11	67.1	1.7
2.5CUR-TPU-Ole-600siRNA NPs	4.3	2.4	55.3	2.7
10CUR-TPU-Ole-600siRNA NPs	13.7	2.3	49.7	10.5
Control L929	5.7	3.4	83.8	7.1
CUR	7.1	1.5	61.2	2.0
siRNA	1.9	1.9	58.4	5.6
TPU-Ole-600siRNA NPs	4.3	0.5	70.2	1.5
2.5CUR-TPU-Ole-600siRNA NPs	1.9	0.8	67.7	1.6
10CUR-TPU-Ole-600siRNA NPs	0.3	0.2	62.9	13.9

Q1: necrotic cells; Q2: late apoptotic cells; Q3: viable cells; Q4: early apoptotic cells.

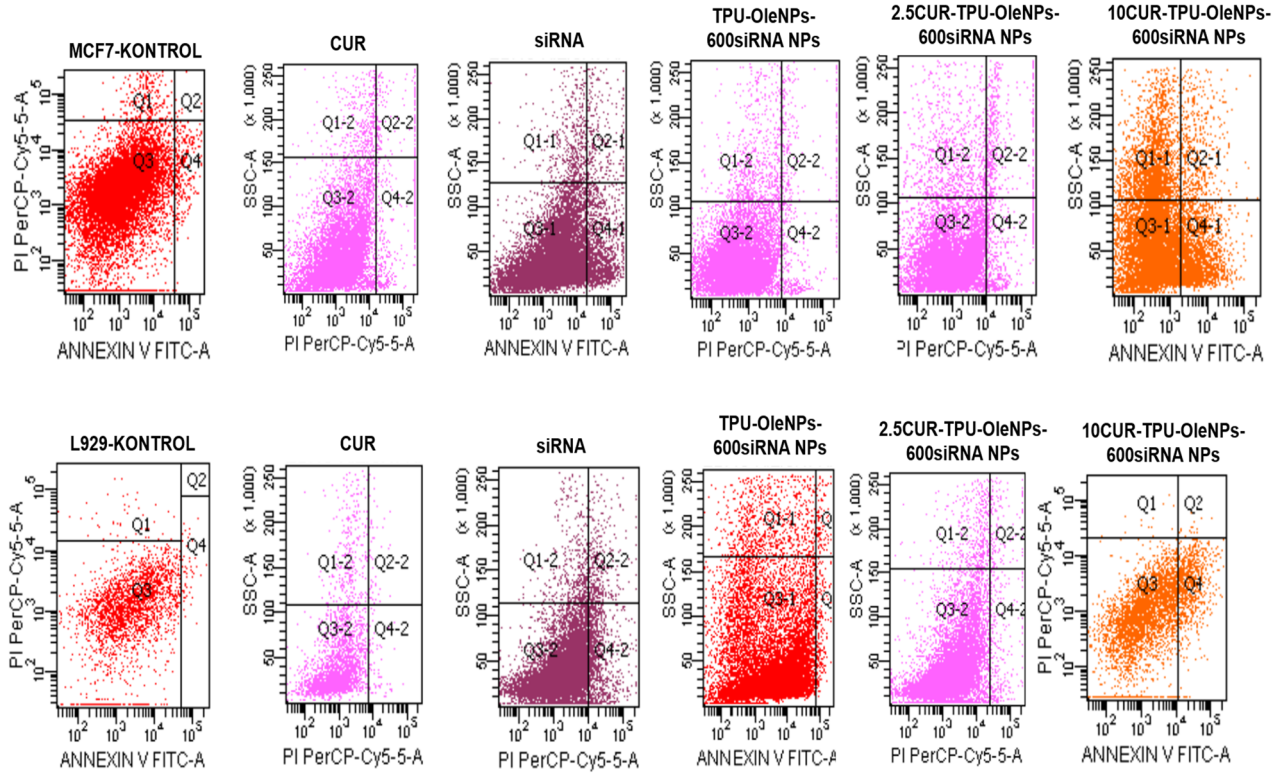

Figure 6. Flow cytometry analysis of apoptosis in L929 and MCF-7 cell lines after treatment with TPU-Ole NPs. Quadrants are labelled as follows: Q1 (necrotic cells), Q2 (late apoptotic cells), Q3 (viable cells), and Q4 (early apoptotic cells). Results are presented as mean ± *SD* ($n = 5$).

MCF-7 breast cancer cells, as evidenced by the lower viability compared to L929 cells, highlighted the specificity and efficacy of this approach. Incorporating siRNA into therapeutic regimens offered a targeted strategy to downregulate oncogenes, thereby enhancing the effectiveness of conventional chemotherapeutic agents. This combination had been shown to overcome drug resistance and reduce the adverse effects associated with high-dose chemotherapy. For instance, a study demonstrated that co-delivery of siRNA targeting the HER2 gene with chemotherapeutic drugs effectively inhibited tumour growth in HER2-positive breast cancer models. Moreover, this combination exhibited significant cytotoxicity in HER-2 positive breast cancer cells, leading to a marked reduction in cell viability (Gu *et al.* 2016**).**

In literature, Sharifiaghdam *et al.* designed a new nanocomplex as an siRNA carrier using a layer-on-layer technique. They prepared this nanocomplex by electrostatically arranging of chitosan and siRNA around the solid core of SeNPs. The percentages of apoptosis and cell viability were investigated in lung cancer (H1299) and embryo-derived fibroblasts (NIH/3T3) in both healthy and cancer cells. According to the results, NIH/3T3 cell viability was 60% when 64 nM siRNA was used, while the apoptosis rate was about 15% (Sharifiaghdam *et al.* 2021). Based on this reference, the 600 nM siRNA concentration used in this study

demonstrated toxic effect to healthy cells and relatively reduced cell viability. Lower cell viability in breast cancer cells was observed for siRNA and CUR combined NPs compared to TPU-Ole NPs. Thanks to the synergistic effect of CUR and siRNA, 10CUR-TPU-Ole-600siRNA NPs especially showed higher rates of early apoptosis and necrosis (10.5% and 13.7%). This result revealed that formulation prepared with 10CUR-TPU-Ole-600siRNA NPs was more effective in silencing cancer cells rather than naked siRNA and CUR. Additionally, the efficiencies of CUR and siRNA released from TPU-Ole NPs were also clearly observed in the results of flow cytometry and confocal microscopy analyses. Supporting this, Zhang *et al* modified the carboxymethyl chitosan polymer with EGFR monoclonal antibody (EGFR) and histidine cholesteryl esters (CHCE). They synthesised CEAM NPs using CHCE, adriamycin, MVP (major vault protein)-siRNA, and (B-cell lymphoma-2) BCL2-siRNA by self-regulation method. Group nomenclatures were designated as CHCE/Adriamycin nanoparticles (CEA NPs), CHCE/Adriamycin/MVP-siRNA NPs (CEAM NPs), CHCE/Adriamycin/BCL2-siRNA NPs (CEAB NPs), and CHCE/Adriamycin/MVP-siRNA/BCL2-siRNA NPs (CEAMB NPs). They investigated the cellular cycle of these self-assembled NPs in oesophageal cancer cells using flow cytometry. According to the results, CEAM NPs and CEAB NPs formulations caused apoptosis in more cells (44.2 and 48.4%) compared to CEA NPs (30.1%). CEAMB NPs caused the most apoptosis (66.2%). These results clearly demonstrated the synergistic effect of adriamycin and siRNA (Zhang *et al.* 2022). Another example was the self-regulated peptide (CPS) nanospheres releasing VEGF siRNA and VEGF antisense oligonucleotides (ASOs) prepared by Panigrahi *et al.* The cellular uptake of siRNA/ASOs, negatively charged macromolecules, was investigated using flow cytometry in HCT-116 human colon cancer cells. CPS-2-mediated cellular release of siRNA was found to be 45.1% for the siRNA loaded group, which was quite high compared to the control. This finding demonstrated the potential of CPS as a carrier (Panigrahi *et al.* 2022).

3.10. Confocal microscopy analysis

Confocal microscopy analysis of MCF-7 cells interacting with TPU-Ole NPs was presented in Figure 7(a). Studies showed that siRNA needed to form an RNA complex in the cytoplasm before silencing specific target genes (Fire *et al.* 1998). Therefore, efficient cellular adhesion and uptake of NPs were essential for the successful intracellular release of siRNA in the cytoplasm (Sun *et al.* 2012). Microscopic images revealed that NP formulations exhibited increased cellular adhesion and they confirmed tumour cell recognition and enhanced intracellular uptake, particularly in siRNA and CUR formulations. Internalisation of siRNA-CUR NPs was observed as green fluorescence localised into the cytoplasm. The fluorescence intensity confirmed that siRNA and CUR were effectively taken up by tumour cells, with the increased green fluorescence indicating successful intracellular delivery. Additionally, the photographs illustrated that siRNA-CUR NPs accumulated in the cytoplasm, where they decomposed and released FAM labelled siRNA into the intracellular matrix. Taken together, these results proposed that siRNA-CUR NPs facilitated the targeted delivery of siRNA into breast cancer cells.

Xia *et al.* prepared RGDfC peptide loaded selenium NPs to produce tumour-targeted gene-releasing vehicles and then modified their nanoformulation with Derlin1-siRNA to silence the Derlin1 gene. RGDfCSe@siRNA showed higher uptake in HeLa cervical cancer cells compared to human umbilical vein endothelial cells (HUVECs). This image confirmed the RGDfC-mediated specific uptake of RGDfCSe@siRNA. RGDfC-Se@siRNA was capable of entering HeLa cells via clathrin-mediated endocytosis and showed faster siRNA release in the cancer cell microenvironment compared to normal physiological conditions (Xia *et al.* 2020).

3.11. Results of RT-PCR

The success of applied gene silencing therapy was also demonstrated by gene expression experiments (Figure 7(b)). C-myc gene expression levels, which were the target of the selected siRNA, were determined by Real-Time PCR experiments with the comparative Ct method. The experimental results proved that the siRNA treatment was successful, and the selected doses of CUR-siRNA NPs were effective in silencing the target cancer gene. It was shown that NPs prepared with the highest dose of siRNA and CUR significantly reduced the expression of the target c-myc gene ($p \leq 0.0001$) (Adnane *et al.* 1989, Liao and Dickson 2000, Hosseini *et al.* 2019). The efficacy of a high CUR dose was compared between formulations containing the different amount of siRNA (100 and 600 nM) and significant differences were found again ($p \leq 0.05$, $p \leq 0.0001$). The success of NPs in gene delivery was demonstrated with the control siRNA group without a carrier and significant difference was determined ($p \leq 0.0001$). Statistical analyses were performed using the Student *t*-test with GraphPad Prism software version 6 (USA). Cases with *p*-values <0.05 were

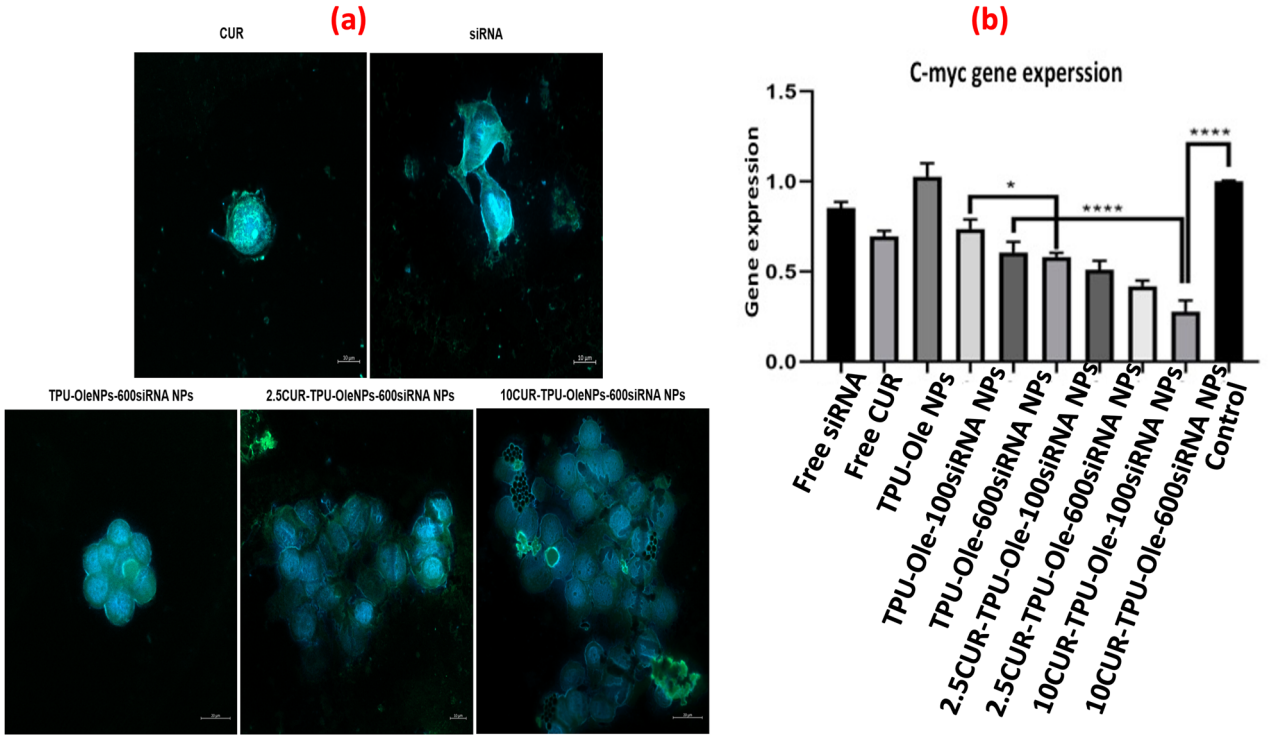

Figure 7. (a) Confocal microscopy images of MCF-7 cells after 24 h incubation with TPU-Ole NPs and free siRNA/CUR. Green fluorescence represents CUR and FAM-labelled siRNA, while blue fluorescence corresponds to the cell nucleus. Scale bar: 20 µm; (b) RT-PCR analysis results following 24 h treatment with all samples. Data are expressed as mean ± *SD* from five independent experiments. Statistical significance: $^{*}p < 0.05$, $^{****}p \leq 0.001$.

considered significant and the significance levels were represented as follows: $p > 0.05$ not significant, as $p \leq 0.05^{*}$, as $p \leq 0.01^{**}$, as $p \leq 0.001^{***}$, and as $p \leq 0.0001^{****}$.

The experimental results demonstrating the successful silencing of the c-myc gene using CUR-siRNA NPs had significant clinical implications for breast cancer therapy. The c-Myc oncogene is known to play a pivotal role in the proliferation and survival of breast cancer cells. Targeting c-Myc expression had been shown to inhibit tumour growth and enhance the efficacy of existing treatments (Habib *et al.* 2020). In a study by Wang *et al.*, RNA interference (RNAi) was utilised to reduce c-Myc expression in MCF-7 breast cancer cells. The results indicated a marked decrease in tumour growth both *in vitro* and *in vivo*, underscoring the therapeutic potential of c-Myc silencing in breast cancer treatment (Wang *et al.* 2005).

Bai *et al.* investigated the silencing of the protein ABCG2 using siRNA as a promising approach to overcome multidrug resistance in cancer cells. For this purpose, adriamycin (ADR) loaded mPEG-PLGA-PLL (PEAL) NPs were used to ensure efficient delivery of ABCG2-siRNA to breast cancer cells. After intravenous injection of siRNA-loaded PEAL NPs into tumour-bearing mice, ABCG2-siRNA-loaded NPs effectively silenced the ABCG2 gene and increased the susceptibility of ADR against MCF-7 cells. As a result, the combination treatment of ABCG2-siRNA with ADR in the presence of a carrier system for the inhibition of human breast cancer cells gave successful results (Bai *et al.* 2015).

3.12. Accuracy research

Standard deviation was calculated for all samples under the defined conditions. The LOD and limit of LOQ were calculated according to the following equations;

$$\text{LOD} = 3.3 \text{ x } \frac{\text{Regression standard error}}{\text{Slope(a)}}$$

$$\text{LOQ} = 10 \text{ x } \frac{\text{Regression standared error}}{\text{Slope(a)}}$$

Conformational analysis results for NPs containing siRNA at pH 5.0 are shown in Table 4. The mean lethal effect of siRNA in 2.5CUR-TPU-Ole-100siRNA NPs; 10CUR-TPU-Ole-100siRNA NPs; 2.5CUR-TPU-Ole-600siRNA NPs; and 10CUR-TPU-Ole-600siRNA NPs was 38.21; 36.81; 36.37; and 32.39 ng/ml, respectively. The standard deviations for these samples were 29.66; 26.93; 29.21; and 24.70, while the LOD-LOQ values were 172.07–521.43; 195.29–612.34; 174.53–523.86;

Table 4. Conformational analysis of siRNA at (a) pH 5.0 and (b) pH 7.4 ($n = 5$).

pH 5.0 (a)	Rate	Mean	Standard deviation (*SD*)	Accuracy or average conversion (%)	RSD (%) (certainty)	LOD	LOQ	R^2	*r* (Correlation coefficient)
TPU-Ole-100siRNA NPs	61.20	34.07	19.20	142.92 ± 170.715	56.34	222.17	673.25	0.931	0.965
TPU-Ole-600siRNA NPs	58.20	30.39	18.88	145.58 ± 187.81	62.131	151.17	458.10	0.967	0.983
2.5CUR-TPU-Ole-100siRNA NPs	95.40	38.21	29.66	106.44 ± 56.29	77.62	172.07	521.43	0.957	0.978
10CUR-TPU-Ole-100siRNA NPs	88.10	36.81	26.93	123.63 ± 126.21	73.15	195.29	612.34	0.946	0.973
2.5CUR-TPU-Ole-600siRNA NPs	92.80	36.37	29.21	104.59 ± 54.14	80.31	174.53	523.86	0.960	0.980
10CUR-TPU-Ole-600siRNA NPs	82.20	32.39	24.70	125.65 ± 112.03	76.28	222.55	674.47	0.931	0.965
pH 7.4 (b)	Rate	Mean	Standard deviation (*SD*)	Accuracy or average conversion (%)	RSD (%) (certainty)	LOD	LOQ	R^2	*r* (Correlation coefficient)
TPU-Ole-100siRNA NPs	55.2	26.04	19.801	114.687 ± 79.203	76.056	198.62	601.883	0.944	0.972
TPU-Ole-600siRNA NPs	49	21.58	16.72	102.316 ± 32.66	77.503	154.607	468.507	0.965	0.982
2.5CUR-TPU-Ole-100siRNA NPs	76.8	36.94	25.23	114.24 ± 79.28	68.31	164.57	498.70	0.961	0.980
10CUR-TPU-Ole-100siRNA NPs	70.4	32.77	23.87	116.94 ± 91.56	72.83	156.34	473.74	0.965	0.982
2.5CUR-TPU-Ole-600siRNA NPs	70.4	34.23	24.54	105.50 ± 34.77	71.69	159.58	483.58	0.963	0.981
10CUR-TPU-Ole-600siRNA NPs	66.4	29.49	22.35	110.33 ± 61.43	75.80	150.81	457.02	0.966	0.983

and 222.55–674.47, respectively. The mean lethal effect of CUR in 2.5CUR-TPU-Ole NPs was only 34.35 ng/ml. The lethality effect increased with 100siRNA. The coefficients and the model were significant (*p*-values <0.5) at a 95% confidence level. According to the results, the lethal effect was higher when siRNA was used in 10CUR-TPU-Ole-100siRNA NPs. The lowest rate of RSD (73.15%) was obtained with 10CUR-TPU-Ole-100siRNA NPs. The killing effect of siRNA in cancer cells increased with siRNA binding.

Conformational analysis results for siRNA at pH 7.4 were also shown in Table 4. The mean lethal effect of siRNA in 2.5CUR-TPU-Ole-100siRNA NPs; 10CUR-TPU-Ole-100siRNA NPs; 2.5CUR-TPU-Ole-600siRNA NPs; and 10CUR-TPU-Ole-600siRNA NPs was 36.94; 32.77; 34.23; and 29.49 ng/ml. The standard deviations of these samples were 25.23; 23.87; 24.54; and 22.35, while the LOD-LOQ values were 164.57–498.70; 156.34–473.74; 159.58–483.58; and 150.81–457.02, respectively. The mean lethal effect of CUR in 2.5CUR-TPU-Ole NPs was 27.42 ng/ml. The lethality effect increased with 100siRNA. The coefficients and the model were significant (*p*-values <0.5) at a 95% confidence level. The lethal effect progressed more slowly and was higher at pH 7.4. As a results, the lethal effect was the highest when 2,5CUR-TPU-Ole-100siRNA was used at pH 7.4. The lowest rate of RSD (68.31%) was obtained with 2,5CUR-TPU-Ole-100siRNA NPs. The killing effect of the therapeutic agent on cancer cells enhanced by siRNA binding at pH 7.4. When the lethal effect in terms of pH examined, it could be said that the optimal pH value was 7.4.

4. Conclusion

The combination of chemotherapeutics offers valuable strategies for overcoming drug resistance and promoting patient recovery. Based on this concept, a highly efficient siRNA-CUR-TPU-Ole nano-carrier system was designed to create a dual-effect carrier. High siRNA binding efficiency was confirmed by the agarose gel electrophoresis. Considering the pH-sensitive release profile, a more rapid and targeted release of CUR and siRNA was observed in acidic environments compared to healthy tissues. Stability tests revealed that the NPs maintained their structural integrity for over a month at pH 5.0 and 7.4. The dual-action system exhibited a significant inhibitory effect on the c-myc gene in MCF-7 cells, attributed to the synergistic effects of siRNA's gene-silencing ability and CUR's anticancer activity. These findings highlighted the novelty of TPU-Ole NPs as a promising pH-responsive and synergistic therapeutic carrier system, offering enhanced tumour suppression compared to free CUR and siRNA.

Disclosure statement

No potential conflict of interest was reported by the author(s).

Funding

This work was funded by TUBİTAK under grant (project no. 221M349); Çankırı Karatekin University Research Fund under grant (Grant no EMY081123B36). The authors extend their appreciation for the financial support provided.

ORCID

Ebru Kilicay http://orcid.org/0000-0002-0042-1417

References

Adnane, J., *et al.*, 1989. Proto-oncogene amplification and human breast tumor phenotype. *Oncogene*, 4 (11), 1389–1395.

Amjed, N., *et al.*, 2022. Preparation and characterization of thermoplastic polyurethanes blended with chitosan and starch processed through extrusion. *International journal of*

biological macromolecules, 208, 37–44. doi: 10.1016/j.ijbiomac.2022.03.008.

Anilmis, M.N., *et al.*, 2019. Designing siRNA-conjugated plant oil-based nanoparticles for gene silencing and cancer therapy. *Journal of microencapsulation*, 36 (7), 635–648. doi: 10.1080/02652048.2019.1665117.

Anita, A., *et al.*, 2014. *In vitro* combinatorial anticancer effects of 5-fluorouracil and curcumin loaded N,O-carboxymethyl chitosan nanoparticles toward colon cancer and *in vivo* pharmacokinetic studies. *European journal of pharmaceutics and biopharmaceutics*, 88, 238–251.

Anitha, A., *et al.*, 2014. Combinatorial anticancer effects of curcumin and 5-fluorouracil loaded thiolated chitosan nanoparticles towards colon cancer treatment. *Biochimica et biophysica acta*, 1840 (9), 2730–2743. doi: 10.1016/j.bbagen.2014.06.004.

Ashrafizadeh, M., *et al.*, 2020. Progress in natural compounds/siRNA co-delivery. Employing nanovehicles for cancer therapy. *ACS combinatorial science*, 22 (12), 669–700. doi: 10.1021/acscombsci.0c00099.

Baby, T., *et al.*, 2021. Microfluidic synthesis of curcumin loaded polymer nanoparticles with tunable drug loading and pH-triggered release. *Journal of colloid and interface science*, 594, 474–484. doi: 10.1016/j.jcis.2021.03.035.

Bai, M., *et al.*, 2015. Enhanced therapeutic effect of adriamycin on multidrug resistant breast cancer by the ABCG2-siRNA loaded polymeric nanoparticles assisted with ultrasound. *Oncotarget*, 6 (41), 43779–43790. doi: 10.18632/oncotarget.6085.

Barick, A.K. and Tripathy, D.K., 2011. Preparation, characterization and properties of acid functionalized multi-walled carbon nanotube reinforced thermoplastic polyurethane nanocomposites. *Materials science and engineering: B*, 176 (18), 1435–1447. doi: 10.1016/j.mseb.2011.08.001.

Barnwell, S.G. and D. Attwood, 1992. Improved oral bioavailability of propranolol in healthy human volunteers using a liver bypass drug delivery system containing oleic acid. *International journal of pharmaceutics*, 88 (1–3), 423–432. doi: 10.1016/0378-5173(92)90342-Y.

Bora, R.S., *et al.*, 2012. RNA interference therapeutics for cancer: challenges and opportunities. *Molecular medicine reports*, 6 (1), 9–15. doi: 10.3892/mmr.2012.871.

Chadar, R. and A. Kesharvani, 2021. Nanotechnology-based siRNA delivery strategies for treatment of triple negative breast cancer. *International journal of pharmaceutics*, 605, 120835. doi: 10.1016/j.ijpharm.2021.120835.

Chevalier, M.T., *et al.*, 2017. Non-covalently coated biopolymeric nanoparticles for improved tamoxifen delivery. *European polymer journal*, 95, 348–357. doi: 10.1016/j.eurpolymj.2017.08.031.

Chow, E.K., *et al.*, 2011. Nanodiamond therapeutic delivery agents mediate enhanced chemoresistant tumor treatment. *Science translational medicine*, 3 (73), 73ra21. doi: 10.1126/scitranslmed.3001713.

Dongsar, T.T., *et al.*, 2023. Emöerging application of magnetic nanoparticles for breast cancer therapy. *European polymer journal*, 187, 111898. doi: 10.1016/j.eurpolymj.2023.111898.

Donsi, F., Wang, Y., and Huang, J.L.Q., 2010. Preparation of curcumin sub-micrometer dispersions by high-presure homogenization. *Journal of agricultural and food chemistry*, 58, 2848–2853.

Elbashir, S.M., *et al.*, 2001. Duplexes of 21-nucleotide RNAs mediate RNA interference in cultured mammalian cells. *Nature*, 411 (6836), 494–498. doi: 10.1038/35078107.

Eljack, S., *et al.*, 2022. Combination of nanovectorized siRNA directed against survivin with doxorubicin for efficient anti-cancer activity in HER2+ breast cancer cells. *Pharmaceutics*, 14 (11), 2537. doi: 10.3390/pharmaceutics14112537.

Farooqi, A.A., Rehman, Z.U., and Muntane, J., 2014. Antisense therapeutics in oncology: current status. *Oncotargets and therapy*, 7, 2035–2042. doi: 10.2147/OTT.S49652.

Fire, A., *et al.*, 1998. Potent and specifc genetic interference by double-stranded RNA in Caenorhabditis elegans. *Nature*, 391 (6669), 806–811. doi: 10.1038/35888.

Gao, C., *et al.*, 2017. pH-responsive prodrug nanoparticles based on a sodium alginate derivative for selective co-release of doxorubicin and curcumin into tumor cells. *Nanoscale*, 9 (34), 12533–12542. doi: 10.1039/c7nr03611f.

Ghaffari, M., *et al.*, 2020. Co-delivery of curcumin and Bcl-2 siRNA by PAMAM dendrimers for enhancement of the therapeutic efficacy in HeLa cancer cells. *Colloids and surfaces. B, biointerfaces*, 188, 110762. doi: 10.1016/j.colsurfb.2019.110762.

Gorzkiewicz, M., *et al.*, 2020. Poly(lysine) dendrimers form complexes with siRNA and provide ıts efficient uptake by myeloid cells: model studies for therapeutic nucleic acid delivery. *International journal of molecular sciences*, 21 (9), 3138. doi: 10.3390/ijms21093138.

Gottesman, M.M., 2002. Mechanisms of cancer drug resistance. *Annual review of medicine*, 53 (1), 615–627. doi: 10.1146/annurev.med.53.082901.103929.

Gu, S., *et al.*, 2016. Therapeutic siRNA for drug-resistant HER2-positive breast cancer. *Oncotarget*, 7 (12), 14727–14741. doi: 10.18632/oncotarget.7409.

Habib, S., Ariatti, M., and Singh, M., 2020. Anti-c-myc RNAi-based onconanotherapeutics. *Biomedicines*, 8, 612.

Hanafi-Boid, M.Y., Ansari, L., and Malaekeh-Nikouei, B., 2016. Codelivery of anticancer drugs and siRNA by mesaporous silica nanoparticles. *Therapeutic delivery*, 7 (9), 649–655. doi: 10.4155/tde-2016-0045.

Hazer, B., *et al.*, 2019. Autoxidized oleic acid bifunctional macro peroxide initiators for free radical and condensation polymerization. Synthesis and characterization of multiblock copolymers. *Journal of polymers and the environment*, 27 (11), 2562–2576. doi: 10.1007/s10924-019-01536-6.

Hosseini, S.A., Zand, H., and Cheraghpour, M., 2019. The ınfluence of curcumin on the downregulation of MYC, insulin and IGF-1 receptors: a possible mechanism underlying the anti-growth and anti-migration in chemoresistant colorectal cancer cells. *Medicina*, 55 (4), 90. doi: 10.3390/medicina55040090.

Kalhapure, R.S. and Akamanchi, K.G., 2012. Oleic acid based heterolipid synthesis, characterization and application in self-microemulsifying drug delivery system. *International journal of pharmaceutics*, 425 (1–2), 9–18. doi: 10.1016/j.ijpharm.2012.01.004.

Kilicay, E., *et al.*, 2016. Concanavaline A conjugated bacterial polyester-based PHBHHx nanoparticles loaded with curcumin for breast cancer therapy. *Journal of microencapsulation*, 33 (3), 274–285. doi: 10.3109/02652048.2016.1169325.

Kim, M., *et al.*, 2023. Co-delivery of curcumin and PTTG1 siRNA by galactose receptor-targeted liposomes for enhanced anti-tumor effects in hepatocellular carcinoma. *Journal of drug delivery science and technology*, 86, 104692. doi: 10.1016/j.jddst.2023.104692.

Layek, B., *et al.*, 2014. Hexanoic acid and polyethylene glycol double grafted amphiphilic chitosan for enhanced gene

delivery: influence of hydrophobic and hydrophilic substitution degree. *Molecular pharmaceutics*, 11 (3), 982–994. doi: 10.1021/mp400633r.

Lee, S.J., *et al.*, 2016. Delivery strategies and potential targets for siRNA in major cancer types. *Advanced drug delivery reviews*, 104, 2–15. doi: 10.1016/j.addr.2016.05.010.

Liao, D.J. and Dickson, R.B., 2000. c-Myc in breast cancer. *Endocrine-related cancer*, 7 (3), 143–164. doi: 10.1677/erc.0.0070143.

Lin, C.Y., *et al.*, 2012. Transcriptional amplification in tumor cells with elevated c-Myc. *Cell*, 151 (1), 56–67. doi: 10.1016/j.cell.2012.08.026.

Lin, J.-T., *et al.*, 2014. Cationic micellar nanoparticles for DNA and doxorubicin co-delivery. *Materials science & engineering. C, materials for biological applications*, 44, 430–439. doi: 10.1016/j.msec.2014.07.049.

Liu, C., *et al.*, 2022. Properties of curcumin-loaded zein-tea saponin nanoparticles prepared by antisolvent co-precipitation and precipitation. *Food chemistry*, 391, 133224. doi: 10.1016/j.foodchem.2022.133224.

Liu, P., *et al.*, 2012. A mPEG-PLGA-b-PLL copolymer carrier for adriamycin and siRNA delivery. *Biomaterials*, 33 (17), 4403–4412. doi: 10.1016/j.biomaterials.2012.02.041.

Liu, Y., *et al.*, 2010. A strategy for precision engineering of nanoparticles of biodegradable copolymers for quantitative control of targeted drug delivery. *Biomaterials*, 31 (35), 9145–9155. doi: 10.1016/j.biomaterials.2010.08.053.

Ma, Z., *et al.*, 2022. Aerosol delivery of star polymer-siRNA nanoparticles as a therapeutic strategy to inhibit lung tumor growth. *Biomaterials*, 285, 121539. doi: 10.1016/j.biomaterials.2022.121539.

Mahdieh, A., *et al.*, 2024. Novel polyurethane-based ionene nanoparticles electrostatically stabilized with hyaluronic acid for effective gene therapy. *Colloids and surfaces. B, biointerfaces*, 236, 113802. doi: 10.1016/j.colsurfb.2024.113802.

Mattu, C., *et al.*, 2013. Comparative evaluation of novel biodegradable nanoparticles for the drug targeting to breast cancer cells. *European journal of pharmaceutics and biopharmaceutics*, 85 (3Pt A), 463–472. doi: 10.1016/j.ejpb.2013.07.016.

McLeod, H.L., 2013. Cancer pharmacogenomics: early promise, but concerted effort needed. *Science*, 339 (6127), 1563–1566. doi: 10.1126/science.1234139.

Medel, S., *et al.*, 2017. Curcumin-bortezomib loaded polymeric nanopartciles for synergistic cancer therapy. *European polymer journal*, 93, 116–131. doi: 10.1016/j.eurpolymj.2017.05.036.

Meng, H., *et al.*, 2013. Codelivery of an optimal drug/siRNA combination using mesaporous silica nanoparticles to overcome drug resistance in breast cancer *in vitro* and *in vivo*. *ACS nano*, 7 (2), 994–1005. 2, doi: 10.1021/nn3044066.

Meng, R., *et al.*, 2021. Preparation and characterization of zein/carboxymethyl dextrin nanoparticles to encapsulate curcumin: physicochemical stability, antioxidant activity and controlled release properties. *Food chemistry*, 340, 127893. doi: 10.1016/j.foodchem.2020.127893.

Meyer, M., *et al.*, 2009. Synthesis and biological evaluation of a bioresponsive and endosomolytic siRNA polymer conjugate. *Molecular pharmaceutics*, 6 (3), 752–762. doi: 10.1021/mp9000124.

Mirza, Z. and Karim, S., 2021. Nanoparticles-based drug delivery and gene therapy for breast cancer: recent advancements and future challenges. *Seminars in cancer biology*, 69, 226–237. doi: 10.1016/j.semcancer.2019.10.020.

Nair, L.S., and Laurencin, C.T., 2007. Biodegradable polymers as biomaterials. *Progress in polymer science*, 32 (8–9), 762–798. doi: 10.1016/j.progpolymsci.2007.05.017.

Omolo, C.A., *et al.*, 2017. Pegylated oleic-acid: a promising amphiphilic polymer for nano-antibiotic delivery. *European journal of pharmaceutics and biopharmaceutics*, 112, 96–108. doi: 10.1016/j.ejpb.2016.11.022.

Panigrahi, B., *et al.*, 2022. Cyclic peptides nanospheres: a '2-in-1' self-assembled delivery system for targeting nucleus and cytoplasm. *European journal of pharmaceutical sciences*, 171, 106125. doi: 10.1016/j.ejps.2022.106125.

Patra, N., Ramesh, P., and Ramanakumar, N., 2024. Oleic-acid-induced changes in the dynamic viscoelastic behavior of poly(methyl methacrylate) polymer film. *Colloids and surfaces A: physicochemical and engineering aspects*, 701 (24), 134889. doi: 10.1016/j.colsurfa.2024.134889.

Qian, J., *et al.*, 2015. Folate-decorated hydrophilic three-arm star-block terpolymer as a novel nanovehicle for targeted codelivery of doxorubicin and Bcl-2 siRNA in breast cancer therapy. *Acta biomaterialia*, 15, 102–116. doi: 10.1016/j.actbio.2014.12.018.

Raja, M.A.G., Katas, H., and Wen, T.J., 2015. Stability, intracellular delivery, and release of siRNA from chitosan nanoparticles using different cross-linkers. *PLOS one*, 10 (6), e0128963. doi: 10.1371/journal.pone.0128963.

Saleh, T., Soudi, T., and Shojaosadati, S.A., 2019. Aptamer functionalized curcumin-loaded human serum albümin (HSA) nanoparticles for targeted delivery to HER-2 positive breast cancer cells. *International journal of biological macromolecules*, 130, 109–116. doi: 10.1016/j.ijbiomac.2019.02.129.

Sarpoli, L.M.G., *et al.*, 2022. Co-delivery of curcumin and Bcl-2 siRNA to enhance therapeutic effect against breast cancer cells using PEI-functionalized PLGA nanoparticles. *Pharmaceutical development and technology*, 27, 785–793.

Sharifiaghdam, M., *et al.*, 2021. Enhanced siRNA delivery and selective apoptosis induction in H1299 cancer cells by layer-by-layer-assembled Se nanocomplexes: toward more efficient cancer therapy. *Frontiers in molecular biosciences*, 8, 639184. doi: 10.3389/fmolb.2021.639184.

Shirangi, A., *et al.*, 2022. Theranostic silk sericin/SPION nanoparticles for targeted delivery of ROR1 siRNA: synthesis, characterization, diagnosis and anticancer effect on triple-negative breast cancer. *International journal of biological macromolecules*, 221, 604–612. doi: 10.1016/j.ijbiomac.2022.09.020.

Sun, Q., Radosz, M., and Shen, Y., 2012. Challenges in design of translational nanocarriers. *Journal of controlled release*, 164 (2), 156–169. doi: 10.1016/j.jconrel.2012.05.042.

Sun, W., *et al.*, 2018. Co-delivery of doxorubicin and anti-BCL-2 siRNA by pH-responsive polymeric vector to overcome drug resistance *in vitro* and *in vivo* HepG2 hepatoma model. *Biomacromolecules*, 19 (6), 2248–2256. doi: 10.1021/acs.biomac.8b00272.

Suo, A., *et al.*, 2017. Folate-decorated PEGylated triblock copolymer as a pH/reduction dual-responsive nanovehicle for targeted intracellular co-delivery of doxorubicin and Bcl-2 siRNA. *Materials science & engineering. C, materials for biological applications*, 76, 659–672. doi: 10.1016/j.msec.2017.03.124.

Suvà, M.L., Riggi, N., and Bernstein, B.E., 2013. Epigenetic reprogramming in cancer. *Science*, 339 (6127), 1567–1570. doi: 10.1126/science.1230184.

Tang, Q. and Gao, K., 2017. Structure analysis of polyether-based thermoplastic polyurethane elastomers by FTIR, ^{1}HNMR and ^{13}CNMR. *International journal of polymer analysis and characterization*, 22 (7), 569–574. doi: 10.1080/1023666X.2017.1312754.

Tang, S., *et al.*, 2015. Inhibition of metastasis and growth of breast cancer by pH-sensitive poly (b-amino ester) nanoparticles co-delivering two siRNA and paclitaxel. *Biomaterials*, 48, 1–15. doi: 10.1016/j.biomaterials.2015.01.049.

Tran, T.T.-D., *et al.*, 2017. Fattigation-platform theranostic nanoparticles for cancer therapy. *Materials science & engineering. C, materials for biological applications*, 75, 1161–1167. doi: 10.1016/j.msec.2017.03.012.

Turino, N., *et al.*, 2021. Positively-charged plasmonic nanostructures for SERS sensing applications. *RSC advances*, 12 (2), 845–859. doi: 10.1039/d1ra07959j.

Vermette, P., *et al.*, 2001. Biomedical applications of polyurethanes. *In*: *Tissue Engineering Intelligence (Unit 6), EUREKAH. COM*. Austin, TX: Landes Bioscience.

Walther, W., and Schlag, P.M., 2013. Current status of gene therapy for cancer. *Current opinion in oncology*, 25 (6), 659–664. doi: 10.1097/CCO.0000000000000004.

Wang, A., *et al.*, 2013b. Temperature- and pH-responsive nanoparticles of biocompatible polyurethanes for doxorubicin delivery. *International journal of pharmaceutics*, 441 (1–2), 30–39. doi: 10.1016/j.ijpharm.2012.12.021.

Wang, B., *et al.*, 2011. Effects of hydrophobic and hydrophilic modifications on gene delivery of amphiphilic chitosan based nanocarriers. *Biomaterials*, 32 (20), 4630–4638. doi: 10.1016/j.biomaterials.2011.03.003.

Wang, L., *et al.*, 2013a. Encapsulation of curcumin within poly(amidoamine) dendrimers for delivery to cancer cells. *Journal of materials science. Materials in medicine*, 24 (9), 2137–2144. doi: 10.1007/s10856-013-4969-3.

Wang, Y.-H., *et al.*, 2005. Knockdown of c-myc expression by RNAi inhibits MCF-7 breast tumor cells growth *in vitro* and *in vivo*. *Breast cancer research*, 7 (2), R220–R228. doi: 10.1186/bcr975.

Woo, J.O., *et al.*, 2014. Development of a controlled release of salicylic acid loaded stearic acid-oleic acid nanoparticles in cream for topical delivery. *TheScientificWorldJournal*, 2014, 205703–205707. doi: 10.1155/2014/205703.

Wu, S., *et al.*, 2018. Synthesis of cationic branched tea polysaccharide derivatives for targeted delivery of siRNA to hepatocytes. *International journal of biological macromolecules*, 118 (Pt A), 808–815. doi: 10.1016/j.ijbiomac.2018.05.221.

Xia, Y., *et al.*, 2020. Functionalized selenium nanoparticles for targeted siRNA delivery silence Derlin1 and promote antitumor efficacy against cervical cancer. *Drug delivery*, 27 (1), 15–25. doi: 10.1080/10717544.2019.1667452.

Yadav, P., *et al.*, 2018. Enhancement of anticancer activity and drug delivery of chitosan-curcumin nanoparticle via molecular docking and simulation analysis. *Carbohydrate polymers*, 182, 188–198. doi: 10.1016/j.carbpol.2017.10.102.

Yalcin, E., *et al.*, 2019. Preparation and characterization of novel albumin-sericin nanoparticles as siRNA delivery vehicle for laryngeal cancer treatment. *Preparative biochemistry & biotechnology*, 49 (7), 659–670. doi: 10.1080/10826068.2019.1599395.

Yamashita, F., *et al.*, 1995. Analysis of *in vivo* skin penetration enhancement by oleic acid based on a two-layer diffusion model with polar and nonpolar routes in the stratum corneum. *International journal of pharmaceutics*, 117 (2), 173–179. doi: 10.1016/0378-5173(94)00327-2.

Yang, X.-Z., *et al.*, 2011. Systemic delivery of siRNA with cationic lipid assisted PEG-PLA nanoparticles for cancer therapy. *Journal of controlled release*, 156 (2), 203–211. doi: 10.1016/j.jconrel.2011.07.035.

Yi, Y., *et al.*, 2019. Glucose-linked sub-50-nm unimer polyion complex-assembled gold nanoparticles for targeted siRNA delivery to glucose transporter 1-overexpressing breast cancer stem-like cells. *Journal of controlled release*, 295, 268–277. doi: 10.1016/j.jconrel.2019.01.006.

Young, S.W., Stenzel, M., and Yang, J.L., 2016. Nanoparticle-siRNA: a potential cancer therapy? *Critical reviews in oncology/hematology*, 98, 159–169. doi: 10.1016/j.critrevonc.2015.10.015.

Zhang, X., *et al.*, 2022. Multifunctional nanoparticles co-loaded with Adriamycin and MDR-targeting siRNAs for treatment of chemotherapy-resistant esophageal cancer. *Journal of nanobiotechnology*, 20 (1), 166. doi: 10.1186/s12951-022-01377-x.

Zhang, Y., *et al.*, 2013. Combinational delivery of c-myc siRNA and nucleoside analogs in a single, synthetic nanocarrier for targeted cancer therapy. *Biomaterials*, 34 (33), 8459–8468. doi: 10.1016/j.biomaterials.2013.07.050.

Zhang, Y., *et al.*, 2016. Co-delivery of doxorubicin and curcumin by pH-sensitive prodrug nanoparticle for combination therapy of cancer. *Scientific reports*, 6 (1), 21225. doi: 10.1038/srep21225.